Tuomas   Valmari

Potassium behaviour during combustion of wood in circulating fluidised bed power plants
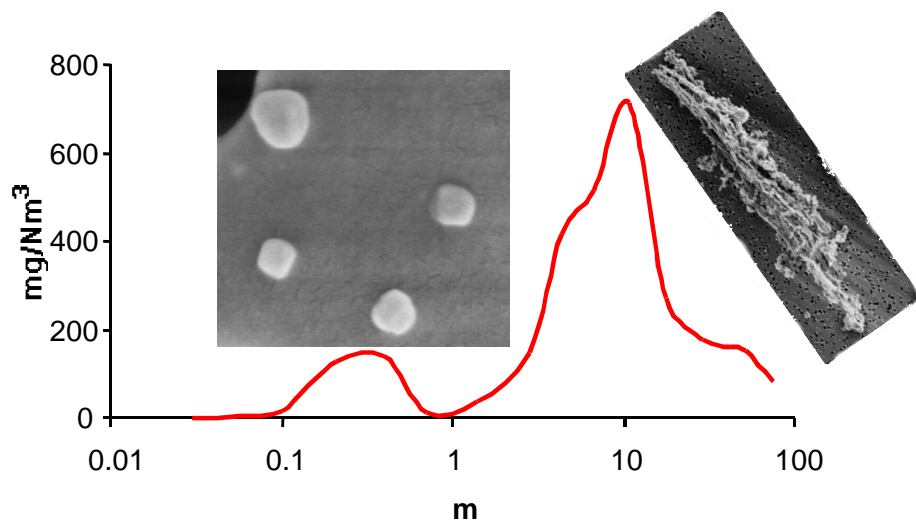
Potassium behaviour during combustion of wood in circulating fluidised bed power plants

Tuomas Valmari

VTT Chemical Technology

VTT

Abstract

The behaviour of alkali metals, especially of potassium, during circulating fluidised bed combustion of wood-based fuels was studied experimentally in pilot-scale and industrial scale combustors. The fuels included willow, forest residue and waste wood co-combusted with paper mill sludge. As a result of this work, the main chemical and physical transformation mechanisms of potassium compounds in the combustion chamber and in the convective pass are presented in this thesis.

Aerosol measurement techniques were used for sampling fly ash and inorganic vapours from the flue gas, upstream and downstream of the convective pass. Samples were collected with cyclones, impactors and filter samplers. Fly ash size distribution was also measured directly in the superheater section with a low-pressure impactor located in-duct in a region where the gas temperature was 650 °C. The method is described and the factors affecting the impactor operation in elevated temperatures are discussed. Elemental analysis methods were used for analysing samples collected by aerosol measurement methods, as well as for conventional samples of fuel, bottom ash and fly ash. Scanning electron microscopy was applied to the fly ash aerosol samples.

Up to 40 % of the ash-forming constituents were retained in the bed and were removed with the bottom ash. The reaction of potassium compounds with quartz sand bed material was found to result in enrichment of K in the bottom ash (relative to Ca) when the fuel Si-content was low (< 0.2 %). The high Si-content (2.6 %) in the fuel resulted in depletion of K in the bottom ash, as the amounts of quartz and silicates in the fuel were large enough for efficient capture of potassium to the ash.

The fly ash released from the combustion chamber consists of i) coarse particles (1–100 μm) that contain all the non-volatile species, including alkali silicates and $CaSO_4$, as well as of ii) sub-micron K_2SO_4 particles. KCl is released from the combustion chamber as vapour.

The fraction of potassium present as sulphates and chlorides was found to be higher the lower the Si to K ratio in the fuel was. The increased amount of Si in the fuel increases the extent of alkali silicate formation, resulting in a decrease in the mass concentrations of K_2SO_4 and KCl. The fine particles included 16–32 % of K (including KCl vapour condensed in the sampling system) when the fuel Si content was < 0.2 %, but less than 1 % of K when the Si content was 2.6 %.

About 60–70 % of the fly ash entering the convective pass was deposited on the heat exchanger surfaces in the convective pass, and was removed during the soot-blowing period. The deposition efficiency correlated clearly with the ash-particle size. The largest particles, including alkali silicates, were deposited most effectively, and the deposition efficiency decreased with decreasing particle size. The deposition efficiency of the fine mode particles, including alkali chlorides and sulphates, was less than about 25 %. The deposition efficiencies of particles with variable compositions, but with the same aerodynamic diameter were not found to be different.

The physical state (vapour, fine particle or coarse particle) of the ash species was shown to have a remarkable effect on the form and rate of ash deposition in the convective pass. When the different fuels were compared, the variation in the deposition efficiency was the most remarkable for sulphur. A majority of the condensed-phase S was present as K_2SO_4 during combustion of willow, resulting in a deposition efficiency of below 20 %. On the other hand, 80 % of the condensed S was deposited during the combustion of forest residue, when 99 % of it was present in the coarse particles as $CaSO_4$.

Preface

This work was carried out at the Aerosol Technology Group (ATG) of VTT Chemical Technology and VTT Energy. I wish to thank the members of the group for the pleasant and supportive athmosphere. The group leaders, Dr. Esko I. Kauppinen and Dr. Jorma K. Jokiniemi are acknowledged for offering me an interesting research subject, and for supervising the work. Professor Rainer Salomaa from the laboratory of Advanced Energy Technologies of Helsinki University of Technology is acknowledged for supervision, especially for comments and suggestions during writing of the thesis. I would like to thank my pre-examiners, Professor Hans Livbjerg and Dr. Kauko Janka for their contribution.

The expertise of Dr. Terttaliisa Lind was invaluable both during the field measurements and during data interpration. The co-operation of Mr. Juha Kurkela is greatly acknowledged, especially during the very first CFBC of wood measurement campaign by ATG in 1994. Dr. Jouko Latva-Somppi is acknowledged for his initiative and enthusiasm, without them the results concerning process D would not exist. Ms. Pirita Mikkanen had a major role in development of high-temperature measurement systems. Dr. Unto Tapper supervised the SEM work. Mr. Jouni Pyykönen, Dr. Kari E.J. Lehtinen, and many other ATG–members gave constructive suggestions to the manuscript. The contributions of Dr. George Sfiris, Ms. Kristina Nilsson and Ms. Annika Johansson were important in the field measurements. Professor Willy Maenhaut and the other people involved in chemical analyses are greatly acknowledged – reliable and accurate elemental analysis results are essential to this thesis.

Especially, I want to thank my parents for their encouragement and support.

Contents

Appendices

     Papers I–VI

Appendices of this publication are not included in the PDF version. Please order the printed version to get the complete publication (http://otatrip.hut.fi/vtt/jure/index.html)

List of symbols and acronyms

<u>Symbols</u>

$BF(X)$	Bed-retention fraction of element X
$BF_{in}(X)$	$BF(X)$ calculated for the ash-forming constituents fed into the combustion chamber
$BF_{out}(X)$	$BF(X)$ calculated for the ash output from the combustion chamber
C	correction due to the temperature-dependence of the ratio of specific heats in equation (25)
C_C	slip correction factor
d	diameter of a spherical particle
d_{ae}	aerodynamic diameter of a particle
d_{ev}	equivalent volume diameter of a particle
D	diffusion coefficient
D_t	heat exchanger tube diameter
k	Boltzmann's constant ($1.38 \cdot 10^{-23}$ J/K)
K	coagulation coefficient
m	mass concentration of particles or of vapour (mg/Nm^3)
m_d	vapour mass concentration corresponding to p_d
m_s	vapour mass concentration corresponding to p_s
m_{ssat}	mass concentration of the supersaturated vapour, $m_{ssat} = m - m_d$
M	particle mass
M_{mol}	molecular weight (kg/mole)
M_{cv}	mass of a condensed vapour
$\dot{m}_d$	mass transfer rate to the surface of a tube by diffusion
$\dot{m}_{th}$	mass transfer rate to the surface of a tube by thermophoresis
N	particle number concentration
N_a	Avogadro's number ($6.02 \cdot 10^{23}$ molecules/mole)
Ncm^3	normalised cubic centimeter (1 cm^3 at 1 bar and 0 °C)
Nm^3	normalised cubic meter (1 m^3 at 1 bar and 0 °C)
p	partial vapour pressure
p_d	saturation vapour pressure on the surface of a fine particle
p_s	saturation vapour pressure
P	pressure

Q	gas mass flow rate
Q_b	bottom ash removal rate
Q_{fl}	fly ash mass flow rate
R	ideal gas constant (8.314 J/(mole · K))
t	time
T	temperature
v	gas volume
V	velocity
Vol	volume
W	impactor stage jet diameter
X	thickness of the thermal boundary layer
•	condensation coefficient
χ	particle dynamic shape factor
∇T	temperature gradient
η	dynamic gas viscosity
λ	gas mean free path
η	dynamic gas viscosity
ρ_g	gas density
ρ_p	particle density
σ	surface tension of a particle

Subscripts

bl	boundary layer
$inlet$	at the inlet of the BLPI
i	BLPI–stage, particle size class
j	impactor jet
p	particle
s	saturation
v	vapour
w	at the tube surface
0	reference conditions, conditions where calibration was carried out
50	corresponding to 50 % cut-diameter
∞	outside the thermal boundary layer

Dimensionless numbers

Nu	Nusselt number, proportional to the ratio of total heat transfer to conductive heat transfer
Pe	Peclet number, proportional to the ratio of bulk mass transfer to diffusive mass transfer
Pr	Prandtl number, proportional to the ratio of momentum diffusivity to thermal diffusivity
Re	Reynolds number, proportional to the ratio of inertial force to viscous force
Sc	Schmidt number, proportional to the ratio of momentum diffusivity to mass diffusivity
Sh	Sherwood number, proportional to the ratio of total mass transfer to diffusive mass transfer
Stk	Stokes number, proportional to the ratio of stopping distance of the particle to the characteristic dimension of the obstacle

Acronyms

BLPI	Berner-type low-pressure impactor
CFBC	Circulating fluidised bed combustion
ESP	Electrostatic precipitator
FAAS	Flame atomic absorption spectroscopy
FBC	Fluidised bed combustion
GFAAS	Graphite furnace atomic absorption spectroscopy
IC	Ion chromatography
ICP-AES	Inductively coupled plasma atomic emission spectroscopy
ICP-MS	Inductively coupled plasma mass spectroscopy
INAA	Instrumental neutron activation analysis
PIXE	Particle-induced X-ray emission
FE-SEM	Field emission scanning electron microscopy
SEM	Scanning electron microscopy

Publications

I   Valmari, T., Kauppinen, E.I., Lind, T., Kurkela, M., Moilanen, A. and Zilliacus, R. (1996). Studies on ash species release during the pyrolysis of solid fuels with a heated grid reactor. In: Applications of Advanced Technology to Ash-Related Problems in Boilers. Ed. by Baxter, L. and DeSollar, R. Proceedings of the Engineering Foundation Conference, Waterville Valley, USA 16–21 July 1995. Plenum Press, New York. Pp. 265–280.

II   Valmari, T., Kauppinen, E. I., Kurkela, J., Jokiniemi, J.K., Sfiris, G and Revitzer, H. (1998). Fly Ash Formation and Deposition During Fluidized Bed Combustion of Willow. *J. Aerosol Sci.*, **29**, pp. 445–459.

III   Latva-Somppi, J., Moisio, M., Kauppinen, E. I., Valmari, T., Ahonen, P., Tapper, U. and Keskinen, J. (1998). Ash formation during fluidized-bed incineration of paper mill waste sludge. *J. Aerosol Sci.*, **29**, pp. 461–480.

IV   Valmari, T., Lind, T.M., Kauppinen, E. I., Sfiris, G, Nilsson, K and Maenhaut, W. (1999). A field study on ash behaviour during circulating fluidized bed combustion of biomass. 1. Ash formation. *Energy and Fuels*, **13**, pp. 379–389.

V   Valmari, T., Lind, T.M., Kauppinen, E. I., Sfiris, G, Nilsson, K and Maenhaut, W. (1999). A field study on ash behaviour during circulating fluidized bed combustion of biomass. 2. Ash deposition and alkali vapour condensation. *Energy and Fuels*, **13**, pp. 390–395.

VI   Lind, T.M., Valmari, T., Kauppinen, E. I., Sfiris, G, Nilsson, K and Maenhaut, W. (1998). Volatilization of the heavy metals during circulating fluidized bed combustion of forest residue. *Environmental Science and Technology*, **33**, pp. 496–502.

Author's contribution

The results described in this thesis are a part of the experimental research work, carried out in the VTT Aerosol Technology Group (VTT Chemical Technology and VTT Energy), concerning ash behaviour in fluidised bed combustion of various wood-based fuels and sludges during 1994–1998. Dr. Esko I. Kauppinen and Dr. Jorma K. Jokiniemi supervised the work. The results presented in this thesis are related to those presented in the doctoral theses of Dr. Jouko Latva-Somppi (1998) and Dr. Terttaliisa Lind (1999). The main contribution of this thesis is the determination of alkali metal transformation mechanisms during circulating fluidised bed combustion of wood, which was carried out by the author based on the results presented in Papers I–VI and on those available in the literature.

Paper I describes a laboratory-scale study on alkali vapour release under oxygen-free conditions. The author of this thesis carried out the aerosol measurements, conducted the data analysis and wrote the paper. Ms. Minna Kurkela operated the experimental system.

Paper II describes results obtained during combustion of willow and wood pellets in a 12 MW pilot-scale plant. The author carried out the work to characterise BLPI-operation at elevated temperatures, carried out the aerosol measurements with Mr. Juha Kurkela, conducted the data analysis, and wrote the paper.

Paper III describes ash behaviour during co-combustion of paper mill sludge and wood-based fuels. Dr. Jouko Latva-Somppi was the main author of this paper. The author of this thesis participated in the measurement campaign, mainly on impactor measurements, and on the interpretation of the results.

Papers IV–VI describe results from the combustion of forest residue in a 35 MW plant. Dr. Terttaliisa Lind and the author carried out the experimental work. The author conducted most of the data analysis and wrote Papers IV and V. Dr. Terttaliisa Lind conducted the data analysis and wrote Paper VI. Paper IV describes results from the combustion of willow in the same plant where the measurements with forest residue took place. The author did not participate in the measurement campaign with willow, but did participate in the data analysis.

1. Introduction

Biomass, in its various forms, is the most common non-fossil source of energy in the world. It was estimated to contribute $55 \cdot 10^{18}$ J, or 15 % of all the primary energy use in 1985 (Hall et al., 1993). The majority of consumption takes place in developing countries for small-scale heating and cooking. In recent decades, biomass and the other renewable energy sources have also become of increasing interest to the industrialised countries. The largest consumer of commercial biomass is the USA, with a consumption of about $4 \cdot 10^{18}$ J per year, contributing 5 % of their total primary energy use (IEA, 1998). Amongst the industrialised countries, the biomass contribution to the total energy consumption is largest in Finland, Sweden and Austria. In Finland, it covered $0.24 \cdot 10^{18}$ J, or 19.2 % of the primary energy consumption in 1998, which is more than any other non-fossil source of energy (nuclear power covered 17.7 %) (Energiakatsaus, 1999). In 1996, largely due to biomass utilisation, the proportions of renewables out of all the energy produced in the European Union member countries were highest in Sweden, Finland and Austria (IEA, 1998). Most of the biomass fuels utilised in Finland are black liquors and other concentrated liquors used by the forest industry. Solid wood-based fuels include predominantly bark and waste wood used by industry. Growth potential for biomass utilisation in Finland exists in industry as well as in the co-generation of heat and power (Helynen and Nousiainen, 1996).

Solid wood-based fuels are most commonly utilised in grate combustion (including stoker-combustion) and fluidised bed combustion. Grate combustors are mainly used in small units (< 5 MW). Fluidised bed combustion (FBC) has become a common technique in the combustion of various solid fuels, mostly in units in the size range of 5–100 MW. Fluidised bed combustors (bubbling FBC and circulating FBC) are suitable for co-generation of heat and power. During co-generation, the efficiency is almost twofold as compared to the generation of power alone.

Fluidised bed combustors are flexible with regard to the fuel used. Most FBC plants are able to utilise different kinds of solid fuels, such as coals, peats, wood-based fuels, sludges and refuse. FBC is especially popular for low-grade fuels, whose utilisation is difficult with other techniques.

The behaviour of the inorganic, ash-forming constituents originating from the fuel has became one of the areas in which the FBC development work is concentrated. This is due to problems caused by the ash in the plant operation, as well as negative environmental and health effects associated with ash. Ash-related problems arise from the tendency of some ashes to adhere to surfaces (Raask, 1985; Anthony, 1995; Baxter et al., 1998). Bed agglomeration occurs when the solid particles in the bed stick to each other, with ash as a bonding agent between the particles. Sintering could result in defluidisation of the bed due to increase in particle size, although in practice sintering is not allowed to continue until defluidisation occurs. Ash deposit growth on heat exchanger surfaces (slagging in the combustion chamber and fouling in the convective pass) causes reduction in heat transfer and promotes corrosion of the heat exchanger material. Large structures formed of ash and bed particles sintered together may cause blocking, especially in the recirculation system (cyclone and return leg) of the circulating FBC.

Sulphate-rich fine particles (< 2.5 µm), formed mainly in various combustion processes, have recently become the subject of studies due to their detrimental health effects. Exposure to sulphate and fine particles has been found to correlate with cancer mortality (Pope et al., 1995). Fine particles are formed from species volatilised during combustion process. The suspected contributors include fine particles formed prior to flue gas release from the stack, as well as fine particles formed in the atmosphere from gaseous SO_2 and NO_x emissions. When compared to coal combustion, SO_2 emissions are usually low during biomass combustion due to low sulphur content in the biomass fuels. However, the concentration of fine particles formed prior to stack release from the plant can be higher than during coal combustion due to a large amount of volatile ash-forming constituents in the biomass. Particles can be removed by, for instance, electrostatic precipitators (ESP), although the particles in the size range of 0.1–1 µm are the most difficult to remove (McElroy et al., 1982; Porle et al., 1995). Once emitted, fine particles can be transported far away from the source (Heyder et al., 1986).

The possibility of using biomass ash, e.g. as a fertiliser, soil conditioner or as an additive to concrete and asphalt, is affected by the properties of the ash. In particular, concentrations of harmful trace elements, such as Cd and Pb, can limit its usability (Linak and Wendt, 1993). Ash formation and behaviour during

the combustion process determines how the harmful constituents are distributed between the different ash fractions, for instance between the large particles collected by the first ESP field and the, on average, smaller particles collected by the downstream fields. The solubility and, in some cases also, the toxicity of the trace elements depend on their chemical form.

The objective of this thesis is to determine the chemical and physical transformation mechanisms of alkali metals (K and Na) during the CFBC of wood-based fuels. The thesis concentrates especially on potassium, as it is usually the most common alkali metal in wood. Alkali compounds, such as KCl and K_2SO_4, are known to be major contributors to fouling and other ash-related problems in CFBC plants (Anthony, 1995; Miles et al., 1996; Baxter et al., 1998; Skrifvars et al., 1998). The main application of the results presented in this thesis is the determination of the factors that affect the quantity, chemical composition and physical form of alkali metals being deposited on the solid particles in the bed, and on the heat exchanger surfaces in the convective pass. The behaviour of other ash species is considered from the point of view of its impact on the behaviour of alkalis.

The research was carried out experimentally, mainly in power plants. Aerosol measurement methods, electron microscopy and elemental analysis methods were applied to ash characterisation. A special effort was put into collecting fly ash samples from flue gas at high temperatures, 650–800 °C, using aerosol sampling techniques. An additional goal of this work was to study the suitability of an in-duct low-pressure impactor sampling technique for fly ash size distribution measurements made directly in the superheater section of a CFBC plant, at a temperature of 650 °C.

The structure of this thesis is as follows. First, a short literature review concerning CFBC technology, ash distribution in the biomass fuels as well as the ash transformations is presented, followed by the introduction of particle and vapour deposition mechanisms, and the role of alkali species in the superheater tube corrosion. The experimental methods are introduced in Chapter 3. A more detailed description of the in-duct impactor technique used in the superheater section is presented, including a discussion on the factors affecting the impactor operation at elevated temperatures. The results of this thesis are summarised in Chapter 4. Ash volatilisation from the fuel in the combustion chamber is

discussed briefly in Section 4.1, based on results of the laboratory-scale experiments. The other results, presented in Sections 4.2–4.6, are based on the pilot and power plant scale measurements. Section 4.2 covers the division of the inorganic constituents into i) a fraction that is retained in the bed and removed with the bottom ash and into ii) a fraction released from the combustion chamber with the flue gas (fly ash, inorganic gases and vapours). The importance of the fuel Si content regarding retention of potassium in the bed is shown. The characteristics of the fly ash and alkali species entering the superheater section are presented in section 4.3, including a discussion on the factors affecting the chemical and physical form of potassium. The deposition efficiencies of the various ash species on the heat exhanger surfaces in the convective pass are discussed in section 4.4. Here the importance of the ash particle size is shown. Discussion on the alkali chloride vapour behaviour (condensation on the fly ash particles and deposition on the superheater surfaces) is presented in sections 4.5 and 4.6. In the final chapter, Chapter 5, the alkali transformation mechanisms during the CFBC of wood, as determined in this thesis, are presented schematically, followed by suggestions for future work.

2. Literature review

2.1 Circulating fluidised bed combustion of biomass

In fluidised bed combustion (Figure 1), the primary combustion air is flowing upwards in a combustion chamber with a velocity sufficiently high for the solid particles to be fluidised in the flow, instead of being pulled down by gravity (see e.g., Kunii and Levenspiel, 1991). A typical fluidisation velocity in circulating fluidised bed combustion (CFBC) is about 5 m/s. This is significantly higher than the minimum velocity required for fluidisation of the solid particles in the bed. The particle suspension is distributed throughout the combustion chamber, with lower particle density higher in the bed. Particles from the dense bottom bed are being continuously carried away with the combustion air. A net flow of particles is transported upwards through the combustion chamber. However, particles are also falling down against the direction of flow, especially near the chamber walls where the gas velocity is lower. This results in a recirculation of particles within the combustion chamber. In FBC, the bed inventory is limited to about 1–2 m in height at rest by the need to limit the pressure drop to 5–15 kPa over the bed (Leckner, 1998).

During the CFBC of biomass the solid inventory in the bed consists of the fuel (which is converted into char and ash), bed material and also, in some cases, sorbent, e.g. limestone. The bed material usually consists of quartz sand particles of 0.3–0.5 mm in diameter. The quartz sand dominates the solid inventory in the bed. A 10–100 MW district heating plant contains tens of tons of sand. The sand is periodically partially replaced to avoid agglomeration of the bed particles. The bed material to be removed (bottom ash) is extracted via the bottom of the bed. Bottom ash contains mainly sand, but also fuel-originated ash attached to the sand particles.

The bed temperature during CFBC of biomass is typically about 800 °C. It is controlled by the heat exchanger surfaces on the combustion chamber walls. The temperature at the top of the bed is higher, by up to ≈ 100 °C, than in the bottom bed. Bed particles absorb the heat generated in combustion and distribute it throughout the furnace by convection and radiation. The temperature on the surfaces of the burning char particles is higher than the gas temperature in the

bed. In the case of FBC of coal, the difference may exceed 200 °C (Hernberg et al., 1993).
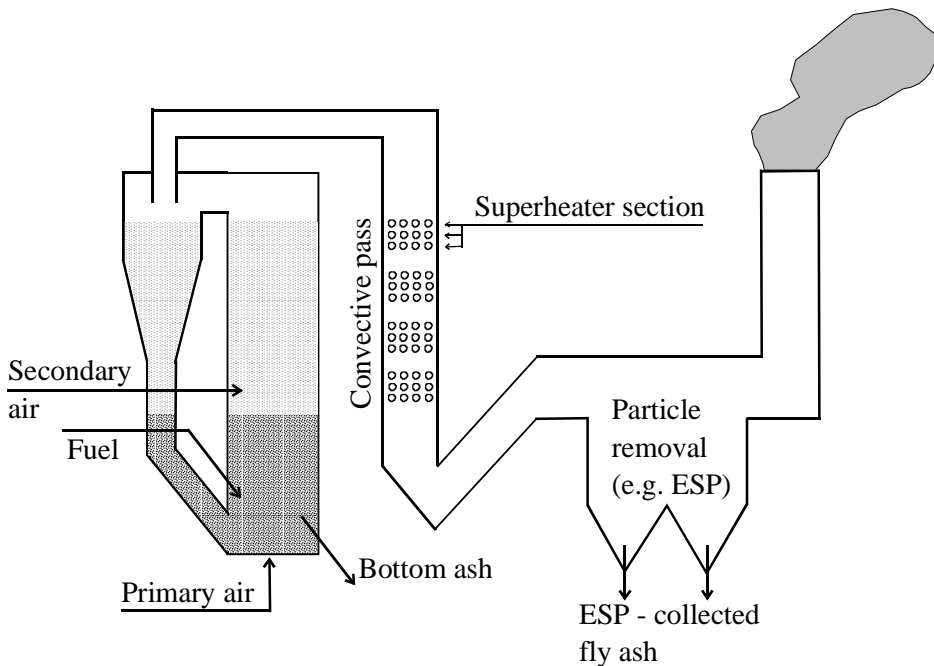
Figure 1. Schematic diagram of a circulating fluidized bed power plant.

The O_2 concentration is low at the dense bottom bed, where a large amount of fuel is competing for the combustion air. At the top of the bed, the concentration of O_2 is higher due to secondary air being introduced above the dense part of the bed, as well as due to lower concentrations of combustible material (Lyngfelt et al., 1996).

The CFB system is equipped with a cyclone located downstream of the combustor. The cyclone recirculates particles larger than the cyclone cut-diameter back to the bed. The recirculated particles include quartz sand particles as well as large char and ash particles. Particles smaller than the cyclone cut-diameter are released with the flue gas as fly ash. Fly ash includes mainly fuel-originated ash, but may include also bed material particles fragmented into a size small enough to avoid recycling. Flue gas is directed through the convective pass where its heat is transferred to steam that flows inside the heat exchanger tubes.

The flue gas temperature is decreased below 200 °C in the convective pass. Fly ash particles are then collected from the flue gas, usually by an electrostatic precipitator (ESP) or a baghouse, before the flue gas is directed through the stack to the atmosphere.

2.2 Ash-forming constituents in biomass fuels

The concentration of the ash-forming constituents (later in this section referred as "ash" for simplicity) and the ash composition depend primarily on the type of the fuel. Based on a principal component analysis, Nordin (1994) classified wood fuel samples including pine, spruce, birch, poplar and oak into categories according to their ash composition. The categories were i) pure wood, ii) branches and logging debris, iii) needles (pine and spruce) and iv) bark. The ash composition varied remarkably between the categories, but not so much within each category despite the variation in the plant species. Pure wood samples had the lowest ash content, < 1 wt-% of the dry fuel. The most common inorganic elements in pure wood were Ca (in average 0.065 wt-% of the dry fuel) and K (0.04 %). The other main elements in descending order were Na, Mg, Cl, S and P.

Due to its importance as a nutrient, potassium is usually the dominant alkali metal in biomass, unlike in coal where sodium dominates. Potassium is bound in biomass predominantly as salts or organically bound in ion-exchangeable form. Alkali metals in biomass are highly volatile during combustion (e.g., Baxter et al., 1998). A minor fraction of silicate-bound alkali metals, especially Na, can also be present. This is the case especially in waste woods and forest residues, where the fuel may include considerable amounts of sand and other impurities. Alkali silicates are considered stable and non-volatile during fluidised bed combustion.

The ash concentrations in the categories ii)–iv) were typically of order of 10 times higher than in the pure wood in the Nordin's study. Ca and K were the most common inorganic elements also in the bark and needle categories. The concentration of Ca was 0.3–0.6 % and the concentration of K 0.16–0.5 % in the wood fuel categories other than pure wood. The young part of the wood (bark, leaves, needles) is richer in potassium than the mature core wood since

potassium tends to move to the young, developing tissues due to its role in the metabolic and transport processes (Bryers, 1996). The core wood has commercial interest other than combustion. For this reason, many wood fuels (e.g., waste wood, bark, forest residue) are depleted in core wood, and enriched with potassium. Fast-growing plants, such as willow (*Salix*), are usually rich in potassium (Nordin, 1994; Bryers, 1996; Baxter et al., 1998). Willow, which is increasingly being cultivated for an energy resource in Sweden, was considered as a separate group in the Nordin's study. The ash concentration in *Salix* samples were about 2 %, and the major inorganic elements were Ca and K. The concentrations of S and Cl in all the wood categories were below 0.1 wt-%.

Si was the dominant element in the debris category (0.5 %), followed by Ca (0.42 %) and K (0.16 %). Although the wood itself is low in Si, the soil components brought in with the debris or forest residue type fuels may include remarkable quantities of silica (Bryers, 1996).

Straws contain typically higher amount of ash-forming constituents, up to 10 %, as compared to the wood-based fuels (Nordin, 1994; Bryers, 1996; Baxter et al., 1998; Sander, 1997). The main inorganic element in straws are Si, K, Ca and Cl. Straws and the other herbaceous fuels may contain significantly higher concentrations of Cl than the wood based-fuels, depending on the amount of Cl present in the nutrients. For instance, Danish straws contain 0.1–1.1 wt-% of Cl, as reported by Sander, 1997. Baxter et al. (1998) and Michelsen et al. (1998) found the combustion of straw to result in much more severe ash-related problems (bed agglomeration, slagging, and fouling) as compared to problems with wood. They associated the problems with high concentrations of volatile alkali metals and chlorine. The concentrations of volatile alkali metals and chlorine in the fuel can be reduced by leaching, especially in the case of straw (Dayton et al., 1999b).

2.3 Ash formation and alkali behaviour during CFBC of biomass

Fuel particles are first dried, as their temperature increases while being fed into the furnace. Biomass fuels may include 50 wt-% of moisture, resulting in about 10 % of H_2O in the combustion gas. After a further increase in temperature, the

hydrogen-rich volatile material is released from the dried fuel, and reacts with oxygen after release. Finally the residual fuel particle, or actually a char particle at this stage, loses the remaining carbon via oxidation at the char surface. During the CFBC of biomass, the final ash includes only minor amounts of unburned carbon. This is partly due to the long residence time of the large char particles that are repeatedly recycled back to the bed by the cyclone (Leckner, 1998).

The volatilisation of potassium was found to take place during the char oxidation stage as KCl, with KOH as secondary volatile species, when switchgrass with a Cl / K molar ratio of 0.5 was burned. In the range of 800–1100 °C, the effect of temperature on the volatilisation of potassium was found to be small (French and Milne, 1994; Dayton et al., 1995). The presence of excess steam shifts the form of the released potassium partly from KCl to KOH when high chlorine containing biomasses are burned. For the low alkali and chlorine containing woody biomasses, the dominant potassium release mechanism was found to be volatilisation or decomposition of K_2SO_4 (Dayton and Milne, 1996). Partial volatilisation of alkali metals was observed to take place during the char oxidation stage also when biomass chars produced from the pyrolysis of pine and switchgrass were burned in a laminar flow reactor at a gas temperature of 1330 °C (Wornat et al., 1995). The alkali metals (Na and K) were volatilised to a larger extent than the divalent and trivalent metals (Mg, Ca and Al).

Alkali metals originally associated with silica-rich grains are not expected to be volatilised, but are retained in the ash particles (Neville and Sarofim, 1985). Also, the organically associated alkali metals may react with the quartz and silicates in the char particle, instead of volatilisation. For instance, only less than 1 % of Na was volatilised in the CFBC of Polish bituminous coal, even if 82 % of Na was water-soluble or ammonium acetate-soluble, i.e. ion-exchangeable (Lind et al., 1994). The fuel-originated ash species attached on bed material will eventually be removed from the bed with bottom ash.

In fluidised bed combustion of biomass, quartz is usually also present in the form of bed material particles. In order for the reaction between alkali compounds and bed sand to take place, the alkali compounds need to be transported on the surface of bed particles. This may take place either via volatilisation followed by diffusion of the gas molecules on the bed particles, or for non-volatilised alkali compounds, via ash particle collision and attachment

on the bed particles. Sodium and chlorine were found to be released disproportionally from NaCl in low rank coals with high sodium, sulphur and chlorine content (Manzoori and Agarwal, 1992; 1993). Sodium formed sodium sulphate on the char surface and was transferred to the surface of the bed material particles, whereas chlorine was not detected on bed material particles.

The alkali vapours (hydroxides and chlorides) are subjected to chemical reactions in the combustion chamber as well as in the convective pass. Reactions of specific interest are those involving formation of alkali sulphates. They are formed via various reactions of alkali compounds (KOH, $NaOH$, KCl and $NaCl$) with SO_2 or SO_3. The generalised forms of these reactions are, in case of potassium compounds:

$$2\ KCl + H_2O + SO_2 + \tfrac{1}{2}\ O_2 \leftrightarrow K_2SO_4 + 2\ HCl, \qquad (1)$$

$$2\ KOH + SO_2 + \tfrac{1}{2}\ O_2 \leftrightarrow K_2SO_4 + H_2O, \qquad (2)$$
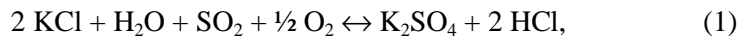
where the corresponding equations for SO_3 can be obtained by replacing $SO_2 + \tfrac{1}{2}\ O_2$ with SO_3. The equations for sodium are similar to those for potassium. It is possible that the alkali sulphate formation is kinetically limited (Steinberg and Schofield, 1990). In fact, the sulphation rate of KCl vapour at 900–1100 ºC was found to be limited by the availability of SO_3 (Iisa et al., 1999). The saturation vapour pressures of alkali sulphates would allow under 1 mg/Nm^3 to be present in the vapour phase at a typical bed temperature (Figure 2). However, the alkali sulphate vapour concentration can be much higher than that if their formation rate is higher than their nucleation and condensation rates (Jokiniemi et al., 1994). SO_2 and SO_3 may also react with Ca-compounds forming condensed-phase calcium sulphate,

$$CaCO_3 \leftrightarrow CaO + CO_2 \qquad (3)$$

$$CaO + SO_2 + \tfrac{1}{2}\ O_2 \leftrightarrow CaSO_4. \qquad (4)$$
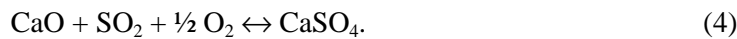
The concentrations of alkali sulphates and $CaSO_4$ in fluidised bed combustion of biomass have been found to be sensitive to the process conditions (e.g., Nordin, 1995). Typical concentrations of alkali chlorides in wood combustion are of the order of milligrams per m^3. In the gas phase they are present as monomers, KCl

24

and NaCl, and as dimers, $(KCl)_2$ and $(NaCl)_2$. Alkali chlorides are condensed at about 600 °C (Figure 2). The condensation thus takes place at the convective pass, either on the ash particles or on the heat exchanger surfaces. According to thermodynamic equilibrium assessments, the presence of alkali hydroxides becomes highly unfavourable when temperature is decreased in the convective pass. The formation of condensed alkali carbonates is predicted when KOH and NaOH are not entirely converted to alkali silicates, chlorides and sulphates. Small concentrations of other compounds, such as alkali nitrates may also be formed.
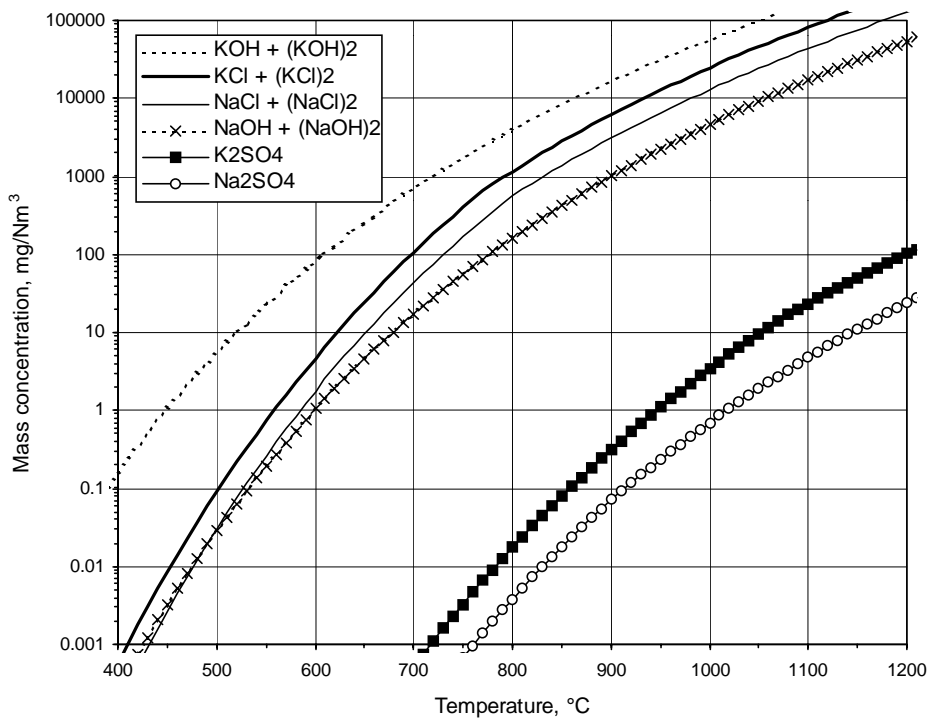

Figure 2. Normalised mass concentrations corresponding to the saturation vapour pressures (m_s at P = 1 bar, equation (8)) of alkali hydroxides, chlorides and sulphates calculated with FACT (Bale et al., 1996). The contribution from monomers and dimers is summed in the case of hydroxides and chlorides. 1 Nm^3 = 1 m^3 at 1 bar and 0 °C.

2.4 Fine particle dynamics during CFBC of biomass

Studies concerning pulverised coal combustion have shown that the fly ash particle size distributions are bimodal (Quann and Sarofim, 1982; Flagan and Seinfeld, 1988; Kauppinen and Pakkanen, 1990). The coarse particle mode, in the super-micron size range, includes, predominantly, species that were not volatilised during the combustion process when the original fuel particles were transformed into ash particles. In fluidised bed combustion, the coarse ash particles are either released from the bed with fly ash (after fragmentation to a size small enough to avoid recirculation), or they end up in the bottom ash after attachment to the bed material particles.

In addition to the coarse mode ash particles, sub-micron fine particles are formed from volatilised inorganic species via homogenous nucleation. In pulverised coal combustion, sub-micron particles are formed from metal oxides (e.g. SiO_2, CaO and MgO) that react with CO under the reducing conditions prevailing at the char surface, forming volatile species (SiO, Ca and Mg). Outside the burning char particle, the conditions are less reducing and the volatilised species are oxidised again. The higher oxides have a low saturation vapour pressure, resulting in formation of high numbers of fine particles via nucleation (Quann and Sarofim, 1982; Neville and Sarofim, 1985). Species that are converted into a condensed phase at lower temperatures may either condense onto the pre-existing particles or surfaces, or form new particles via nucleation.

The nucleation rate (number of particles formed in unit time and unit volume) is strongly correlated with the saturation ratio, defined as p/p_s. The partial pressure of a given vapour may exceed p_s either due to a decrease in temperature, or as the consequence of a chemical reaction where a compound with a high p_s is converted to one with a lower p_s. To a good approximation, the nucleation rate is negligible until a critical saturation ratio is reached, after which the particle formation is rapid. The partial vapour pressure drops to p_s, as the newly formed particles quickly scavenge the vapour. The value of the critical saturation ratio depends on the substance and on the temperature.

The mass growth rate (kg/s) of an aerosol particle with a diameter smaller than the gas mean free path (λ), due to vapour condensation can be presented as (Seinfeld and Pandis, 1998; Hinds, 1999),

$$\frac{dM}{dt} = \frac{\pi d^2 \alpha (p - p_d)}{\sqrt{2\pi k T N_a / M_{mol,v}}}, \quad d < \lambda, \tag{5}$$

$$p_d = p_s \cdot \exp\left(\frac{4\sigma \cdot M_{mol,p}}{d \cdot R \cdot T \cdot \rho_p}\right), \tag{6}$$

$$\lambda = \frac{T}{293\text{K}} \cdot \frac{1\,\text{bar}}{P} \cdot 0.066\,\text{ìm} \quad \text{for air}, \tag{7}$$

where M is the particle mass, t is the time, d is the particle diameter (the particle is assumed to be spherical), p is the partial vapour pressure, p_d is the saturation vapour pressure on the surface of the particle, k is Boltzmann's constant ($1.38 \cdot 10^{-23}$ J/K), N_a is Avogadro's number ($6.02 \cdot 10^{23}$ molecules/mole), $M_{mol,v}$ and $M_{mol,p}$ are the molar weights of the vapour and of the substance of the particle, respectively (kg/mole), T is the temperature, m_v is the mass of the vapour molecule, p_s is the saturation vapour pressure on a flat surface (or on a large aerosol particle), σ is the surface tension of the particle (N/m), R is the ideal gas constant (8.314 J/(mole·K)), ρ_p is the particle density, and P is the actual pressure. The condensation coefficient • is the fraction of arriving vapour molecules that stick to the particle. There is uncertainty about the correct value of • , values from 0.04 to 1 have been suggested (Seinfeld and Pandis, 1998; Hinds, 1999). The vapour mass concentration m (mg/Nm^3) is related to p by

$$m = \frac{M_{mol,v}}{R \cdot T_0} \cdot \frac{P_0}{P} p \tag{8}$$

where T_0 and P_0 are the standard temperature and pressure respectively. The vapour mass concentrations corresponding to p_s and p_d (m_s and m_d) are obtained from equation (8) where p is replaced by p_s and p_d, respectively. In this thesis, the mass concentrations of vapours and of particles are given at $T_0 = 273$ K and $P_0 = 1$ bar. Thus, a normalised cubic meter (1 Nm^3) refers to 1 m^3 at 1 bar and 0 °C.

The evaporation from the particle surface compensates for the vapour condensation on the particle if $p = p_d$. Net condensation occurs if $p > p_d$. In the

case of more than one vapour species condensing at the same time, p_d is smaller than the value given by equation (6), as the evaporation rate of each species is decreased by the other species that are partially covering the particle surface. The mass growth rate of particles with $d > \lambda$ is smaller than the one given by equation (5), since the vapour pressure is decreased around the particle, which is acting as a vapour sink.

The number of particles is decreased and the particle size increased by coagulation. The number of monodisperse particles under influence of coagulation is decreased at the rate of

$$\frac{dN}{dt} = -KN^2 , \qquad\qquad (9)$$

where N is the particle number concentration and K is the coagulation coefficient (Hinds, 1999). The value of K depends on temperature, particle size and gas viscosity (Seinfeld and Pandis, 1998). The fine fly ash particle concentrations measured downstream of the convective pass in various combustion processes are of the order of 10^7–10^8 particles/cm^3 in cases where a significant fraction of the ash is volatilised (Lind et al., 1996; Christensen and Livbjerg, 1996; Christensen et al., 1998). Apparently the coagulation rate, rather than the nucleation rate, is the factor limiting the fly ash particle concentration, if the initial concentration was greater than about 10^8 particles/cm^3. For instance, consider a case of 100 mg/Nm^3 of fine particles with a density of that of alkali suphates (2.7 g/cm^3) formed by nucleation at $t = 0$. At 600 °C, coagulation limits the concentration down to 10^9 particles/cm^3 in less than half a second, no matter how high the number concentration was at $t = 0$. The fine particles coagulate predominantly with other fine particles, even if the coagulation coefficient is higher for the coagulation between a fine and a coarse particle than for coagulation between two fine particles. This is because the number concentration of coarse particles is typically several orders of magnitude lower than that of fine particles.

2.5 Ash deposition on the heat exchanger surfaces in the convective pass

In the convective pass, heat carried by the flue gas is collected by steam flowing inside the heat exchanger tubes. The tubes usually have a circular cross-section and are located perpendicular to the flow. The heat exchangers in the convective pass are arranged as sections. The flue gas temperature is decreased down to about 600 °C at the superheater section. The flue gas temperature downstream of the convective pass is below 200 °C.

2.5.1 Transport to the tube surface

Fly ash particles and inorganic vapours are transported to the heat exchanger surfaces via various mechanisms. The most important mechanisms include vapour diffusion followed by condensation, thermophoretic deposition of sub-micron particles, and impaction of super-micron particles (Raask, 1985; Rosner, 1986; Jokiniemi et al., 1996). In the following, the mass transfer rates ($\dot{m}$, kg/m^{2}s) of the ash-forming constituents to the heat exchanger tube surface via different mechanisms are discussed.

Diffusion. Diffusion is the net transport of particles and gas molecules from an area of high gas concentration towards an area of lower concentration by Brownian motion. The concentrations of the condensing vapours and of the depositing particles are depleted in the neighbourhood of an obstacle, such as a heat exchanger tube, which is acting as a sink.

The mass transfer rate to the tube surface by diffusion ($\dot{m}_d$) can be estimated from

$$\dot{m}_d = \frac{D \cdot \mathrm{Sh}}{D_t} m ,\qquad (10)$$

where D is the diffusion coefficient, Sh is the Sherwood number, D_t is the tube diameter and m is the mass concentration of the vapour (in equation (10) m_s is assumed to be negligible compared to m), or of the particles (Rosner, 1986; Sarofim and Helble, 1994). The Sherwood number (Sh) is typically evaluated

assuming that there is an analogy between mass transfer and heat transfer (Rosner, 1986),

$$Sh = f(Re, Sc),$$
$$Nu = f(Re, Pr),$$
(11)

where the function f is the same for Sh and Nu.

$$Re = \frac{\rho_g V D_t}{\eta},$$
(12)

$$Sc = \frac{\eta}{\rho_g D},$$
(13)

where Re is the Reynolds number, Sc is the Schmidt number, Nu is the Nusselt number, Pr is the Prandtl number (Pr $\approx$ 0.7 for air), η is the dynamic gas viscosity, ρ_g is the gas density and V is the gas velocity. The function f in equation (11) is the same for Sh and Nu. The value of Nu can be found from empirical correlation for a circular cylinder in cross flow (Perry's..., 1984),

$$Nu = a \cdot Re^b \, Pr^{1/3},$$
$$a = 0.683 \text{ and } b = 0.466, \text{ when } 40 < Re < 4000.$$
(14)

Using equations (10) – (14), Sh and $\dot{m}_d$ can be presented as

$$Sh(Re, Sc) \approx 0.683 \cdot Re^{0.466} \cdot Sc^{1/3}, \ 40 < Re < 4000$$
(15)

$$\Rightarrow \dot{m}_d \approx 0.683 \cdot Re^{0.466} \cdot \frac{D^{2/3} \cdot \eta^{1/3}}{D_t \cdot \rho_g^{1/3}} m, \ 40 < Re < 4000.$$
(16)

Diffusion is an important transfer mechanism mainly for vapours, since the diffusion coefficient decreases rapidly as the size of the diffusing object increases. For instance, in air at 650 °C, $D = 7 \cdot 10^{-5}$ m^2/s for KCl-vapour molecules, $D = 2 \cdot 10^{-7}$ m^2/s for unit-density ($\rho = 1$ g/cm^3) aerosol particles with

$d = 0.01$ μm and $D = 3 \cdot 10^{-9}$ m²/s for unit-density particles with $d = 0.1$ μm, as calculated using the Stokes-Einstein equation (Hinds, 1999).

Thermophoretic deposition. An aerosol particle experiences collisions with gas molecules. A net force is exerted on a particle located in a temperature gradient (Hinds, 1999). This is because the gas molecules on the hot side of the particle have, on average, more kinetic energy compared to those on the cold side. Thus, they can push the particle towards the cold region more effectively than the molecules on the cold side can withstand. The thermophoretic velocity is independent of particle size for particles with $d < \lambda$,

$$V_{th} = \frac{-0.55\eta}{\rho_g} \cdot \frac{\nabla T}{T} , d < \lambda , \qquad (17)$$

where ∇T is the temperature gradient (Waldmann and Schmitt, 1966). The thermophoretic velocity decreases with increasing diameter when $d > \lambda$, because there is a temperature gradient within the particle that decreases the temperature gradient in the gas in the immediate vicinity of the particle.

The thermal gradient prevailing in the thermal boundary layer of the tube can be estimated from

$$\frac{\nabla T}{T} \approx \frac{\mathrm{Nu(Re, Pr)}}{D_t} \cdot \frac{T_\infty - T_w}{T_w} , \qquad (18)$$

where T_∞ is the gas temperature outside the thermal boundary layer and T_w is the temperature at the tube surface (Rosner, 1986). The mass transfer rate of sub-micron particles to the tube surface by thermophoresis ($\dot{m}_{th}$) is of the order of

$$\dot{m}_{th} \approx \dot{m}_d \cdot \frac{\mathrm{Pe}}{1 - e^{-\mathrm{Pe}}} , \qquad (19)$$

$$\mathrm{Pe} = \frac{|V_{th}| D_t}{D \cdot \mathrm{Sh}} \approx \frac{0.55\eta}{D\rho_g} \frac{(T_\infty - T_w)}{T_w} \left(\frac{\mathrm{Pr}}{\mathrm{Sc}} \right)^{1/3} , \mathrm{Pr} \approx 0.7 \text{ for air,} \quad (20)$$

where Pe is the Peclet number (Rosner, 1986). In the typical case of Pe $\gg$ 1, the equation for $\dot{m}_{tb}$ can be further simplified,

$$\dot{m}_{tb} \approx \dot{m}_d \cdot \text{Pe}$$

$$\approx \frac{0.33 \cdot \eta}{\rho_g D_t} \text{Re}^{0.466} \frac{(T_\infty - T_w)}{T_w} m, \tag{21}$$

$$d < \lambda, \ \text{Pe} \gg 1, \ 40 < \text{Re} < 4000 \ \text{and} \ \text{Pr} = 0.7.$$

The thermophoretic deposition rate is highest on a clean tube surface, as the temperature gradient between the surface and the flue gas is then the steepest. The growth of the thermal insulating deposit layer increases the outer-surface temperature, decreasing the temperature gradient (Bryers, 1996).

Impaction. Impaction is initiated by gas flowing towards a surface. As the flow is finally turned away to bypass the obstacle, coarse particles are not able to follow the flow due to their inertia, but continue their motion towards the surface. Inertial impaction is a term used to describe impaction from the main flow that is curved, for instance to bypass a heat exchanger tube. In turbulent eddy impaction, the particles are driven towards surfaces by turbulent eddies. To become deposited, the particle must have enough inertia to penetrate through the laminar boundary layer surrounding the target. The impaction on the heat exchangers in the flue gas ducts is a combination of these two mechanisms.

The most important parameter affecting the impaction efficiency (the probability that a particle originally moving towards the tube will actually hit the tube), is the particle Stokes number (Stk) (Hinds, 1999),

$$\text{Stk} = \frac{\rho_p d^2 V}{9\eta D_t}. \tag{22}$$

Here the slip correction factor is neglected, as it is important only for particles below 1 μm in diameter. The property of the particle related to the impaction efficiency is the aerodynamic diameter d_{ae}. In super-micron size range, d_{ae} can be calculated from equation (23).

$$d_{ae} = d\sqrt{\frac{\rho_p}{1\,\text{g/cm}^3}},\, d > 1\grave{\text{i}}\,\text{m}. \tag{23}$$

Particles with Stk < 0.125 are not deposited via inertial impaction (Wessel and Righi, 1988). However, they may become collected via turbulent eddy impaction (Pyykönen et al., 1997). Stk < 0.125 corresponds to d_{ae} smaller than $\approx$ 10–20 µm when V, η and D_t are given values typical at the superheater section. The impaction efficiency exceeds 50 % at Stk $\approx$ 1.5, corresponding to $d_{ae} \approx$ 50 µm (Wessel and Righi, 1988). The particle-size dependence of the deposition rate on the leeward side and on the tubes behind the first row of tubes is not as straightforward as it is for the fronts of the first row of tubes. The largest particles are depleted on the leeward side, since they are not able to follow the curved streamline around the obstacle.

An example. Typical flow conditions in the superheater section of the CFBC plant include $V \approx$ 10 m/s, $T_\infty \approx$ 850 °C upstream of the superheater section, $T_w \approx$ 550 °C, $\rho_g \approx$ 0.3 kg/m³, η $\approx$ 4 · 10^{-5} Ns/m² and $D_t \approx$ 4 cm. Under the given conditions, Re = 3000.

Consider a case of flue gas containing 10 mg/m³ of alkali chloride vapour, 10 mg/m³ alkali sulphate fine particles and 1000 mg/m³ of coarse fly ash particles. The mass transfer rate of alkali chloride vapour to the tube surface is 0.6 mg/m²s, as calculated from equation (16) using $D = 7 \cdot 10^{-5}$ m²/s. It should be noted that the vapour condensation on the tube surface only takes place to a significant extent in a narrow temperature range. T_∞ must be high enough so that a considerable fraction of the alkali chloride is still in the vapour phase, yet T_w must be below the dew point. The vapour may nucleate or be condensed on the fly ash particles also in the thermal boundary layer of the superheater tube. This results in a decrease of the mass transfer rate of the volatilised species, in extreme cases down to the same value as if the species had been originally present in a condensed form (Castillo and Rosner, 1988). A rough estimate of the decrease in the mass transfer rate due to vapour nucleation or condensation taking place already prior to the thermal boundary layer can be obtained using equations (16) and (21),

$$\frac{\dot{m}_{th}}{\dot{m}_{d,v}} \approx 0.49 \cdot \mathrm{Sc}_v^{2/3} \left(\frac{T_\infty - T_w}{T_w} \right), \tag{24}$$

where the subscript v refers to vapour. In the present example, $\mathrm{Sc}_v = 1.9$ for KCl vapour molecules, and $\dot{m}_{th}/\dot{m}_{d,v} \approx 0.4$. The mass transfer rate of the alkali sulphate fine particles in the present example is 0.25 mg/m^{2}s.

Under the conditions in the present example, a piece of tube with a cross-section of 1 m^2 is exposed to 10 m^3 of flue gas/second. With an impaction efficiency of, say 20 %, the mass transfer rate of the coarse particles onto the front of the first row of tubes would be 2000 mg/m^{2}s.

The calculated mass transfer rates of the alkali chlorides and sulphates are of realistic order of magnitude, resulting in a deposit growth rate of the order of 0.01 mm/day. On the other hand, the deposit layer on the front of the first row of tubes would grow by an order of 10 cm/day due to impaction of coarse particles. It is obvious that such a particle construction is not stable, but a majority of the impacted coarse particles must either bounce away immediately after collision, or later fall off the tubes.

2.5.2 Attachment on the surface

Deposition results if a particle or a vapour molecule transported to the tube surface also sticks onto the surface. Vapour molecules, driven by thermophoresis and Brownian diffusion, are able to penetrate through the pores of the pre-existing layer of deposited particles towards the innermost layer. Alkali chlorides are condensed at about 600 °C (Figure 2), enabling them to diffuse through the deposit layer towards the cooled superheater tube until the temperature is decreased enough for condensation. Alternatively, a chemical reaction between the vapour and surface material may result in deposition.

Particles larger than about 10 μm have been found to have enough kinetic energy to re-entrain back to the flue gas flow in pulverised coal-fired boilers (Raask, 1985). Smaller fly ash particles have a higher sticking efficiency. The sticking efficiency depends on the surface properties of the particle and of the target. A surface layer formed of low-viscosity (especially liquid-phase) material

promotes sticking. The material on the deposit layer may form a solution whose melting point is much lower than that of the pure species. Alkali sulphates and chlorides are known to decrease the viscosity and melting point of the ash mixtures. Deposition of sub-micron alkali-rich particles or condensation of alkali vapours on the heat exchanger surface may create a sticky layer that promotes coarse particle retention on the deposit layer. For this reason, the innermost deposit layer is often depleted of particles larger than 10 μm, that are retained in the surface only after the initial sticky layer is formed (Bryers, 1996; Miles et al., 1996; Jensen et al., 1997; Baxter et al., 1998).

Michelsen et al. (1998) studied deposit formation during combustion of straw with flue gas temperatures of 720 to 750 °C. The innermost deposit layer consisted of KCl condensed on the tube surface. Impacted fly ash particles were observed outside the KCl-rich layer. The KCl-layer was denser and thicker when the deposition probe temperature was 550 °C (20–30 μm) compared to the case when the probe temperature was 460 °C (5–10 μm). Molten phases were present in the innermost layer at 550 °C, but not at 460 °C.

The fly ash deposits are periodically removed from the heat exchanger surfaces by soot-blowing, which is usually carried out by directing a high velocity steam jet against the heat exchanger tube surface. The deposit becomes problematic if it is too tenacious to be removed. The outer deposit layer is usually easily removable, but this is not necessarily the case with the innermost alkali-rich layer. The tenacity of the biomass ash is difficult to predict and is usually determined empirically (Miles et al., 1996; Baxter et al., 1998). Jensen et al. (1997) found that the superheater deposit was harder and more difficult to remove in straw-fired boilers if it was directly condensed on the surface or partially melted. The fraction of hard deposit was higher when the sulphur content in the deposit was high.

2.6 Corrosion of the superheater tubes

The temperature of the flue gas entering the superheater section in the CFBC of biomass is about 800 °C. The exit temperature of the steam flowing inside the heat exchanger tubes is typically about 500 °C. The thermal efficiency of the process could be increased by elevating the steam temperature, but the

temperature is limited due to corrosion of the superheater tubes (Miles et al., 1996; Michelsen et al., 1998).

Sulphur and chlorine accelerate the corrosion in combustion systems. The corrosion rate due to the influence of molten sulphates is the highest in the temperature range of approximately 600–700 °C (Raask, 1985). Chlorine-induced corrosion is considered the most severe mechanism at the lower superheater temperatures typical for biomass combustion. Gaseous chlorine compounds (HCl and Cl_2) penetrate through the metal oxide layer on the tube surface and react chemically with iron and chromium present in the steel, forming volatile $FeCl_2$ and $CrCl_2$ (Raask, 1985; Michelsen et al., 1998). Metal chloride vapour is oxidised, forming a non-protective layer, as it diffuses from the reducing tube interior to the area where more oxygen is available.

According to experience with kraft recovery boilers, the superheater corrosion can be minimised by keeping the tube surface temperature below the point where partial melting of the deposit begins (Tran, 1997). Molten deposits are corrosive, because molecules are more mobile (higher diffusion rate) in liquids than in solids. Also, liquids may remove corrosion products from the tube surface by dissolution. In the study by Michelsen et al. (1998), the corrosion rates of the samples set to 550 °C (molten phases were observed next to the steel surface) were much larger than those of the ones kept at 460 °C (no molten phases close to the steel surface).

The most commonly proposed sources of the corrosive chlorine compounds include i) HCl and Cl_2 from the flue gas and ii) condensed-phase KCl and NaCl (Raask, 1985; Michelsen et al., 1998; Nielsen et al., 1999). In the latter case, alkali chlorides react with SO_2 or SO_3 within the deposit, resulting in the formation of alkali sulphate and HCl or Cl_2. Condensed, or deposited, alkali chlorides have a much longer interaction time with the steel surface than the chloride vapour-molecules that bounce back from the surface if they do not react immediately. The time for this reaction to take place is long, the deposited ash may have to wait 1–2 days for soot-blowing, and yet the tenacious part of the deposit may not be removed by soot-blowing.

3. Methods

3.1 Power plants and fuels

The laboratory-scale experiments were carried out using two kinds of wood chips. They included chips made out of unfractionated wood, as well as chips enriched with bark, a residue obtained when raw material for the pulp industry is produced. The heated grid reactor and the experimental set-up is described in Paper I.

The measurements in the pilot and industrial scale plants (Papers II–VI) were carried out in the following four processes:

A) Combustion of willow (Salix) supplemented with 20 wt-% of wood pellets in a pilot-scale plant at Chalmers University, Gothenburg, Sweden. The measurements were carried out for 4 days in December 1994.

B) Combustion of willow (Salix) in a 35 MW power plant located in Nässjö, Sweden. Willow was burned during the daytime, forest residue was burned at night. Measurements were carried out for 3 days in March 1997.

C) Combustion of forest residue in the same unit as the one in Process B. Measurements were carried out for two days in April 1996.

D) Co-combustion of paper mill sludge and waste wood in an industrial plant. The measurements were carried out throughout one week in May 1995. The measurements were a part of a project where co-combustion of sludges and wood-based fuels were studied in circulating and bubbling fluidised beds (Latva-Somppi, 1998).

The process conditions and fuel analysis results are summarised in Table 1. Bed temperatures were about 800 °C in all the cases. Processes with willow as the major fuel (A and B) showed significantly high CO-concentrations in flue gas, indicating non-optimal carbon conversion.

Table 1. Process conditions during the circulating fluidised bed combustion processes studied.

Process	A	B	C	D
Fuel	Willow and wood pellets	Willow	Forest residue	Paper mill sludge and waste wood
Publication	II	IV	IV – VI	III
Thermal input, MW	8–9	24	23	19
Bed temp., °C	830–845	760–780	750–830	765
Fuel feed (dry), kg/h	1800	4700	5200	5500
Ash feed with fuel, kg/h	32	80	110	750
Sand feed, kg/h	n.a.	10–60	230–280	about 40
Fuel moisture, %	About 50	51–52	44–49	44
Concentration in dry fuel, %:				
C	50	50	52	43
H	6.2	6.2	6.3	5.4
N	0.5	0.4	0.6	0.5
Ash	1.8 [a]	1.7	2.1	13.6 [a]
Ca	0.46	0.36	0.44	2.6
Si	0.07	0.036	0.17	2.6
P	0.07	0.08	0.046	0.044
K	0.23	0.24	0.15	0.16
Na	0.007	0.007	0.017	0.09
S	0.06	0.03	0.04	0.36
Cl	0.02	0.01	0.025	< 0.1
Flue gas, %:				
O_2, %	4	4–5	3–4	3–4
CO, ppm	> 5000	> 500	100 – 200	n.a.
SO_2, ppm	n.a.	9–12	6–7	n.a.
Aerosol sampling:				
Upstream of the convective pass	Yes [b]	Yes	Yes	No
Downstream of the convective pass	Yes	Yes	Yes	Yes

[a]) 95 % of ash originates from willow (Process A) and 70 % from waste wood (Process D).

[b]) Sampling in the convective pass (flue gas temperature 650 °C).

The concentration of alkali metals (K+Na) was roughly similar in all the fuels studied (0.17–0.25 wt-% of the fuel). Ca was the most common inorganic element in all the fuels. The overall ash concentration was about sevenfold in the mixture of sludge and wood when compared to the other fuels. The variation in Si-concentration was significant between the fuels, varying from 0.04 % in the willow to 2.6 % in the mixture of sludge and wood. The concentrations of S and Cl were of the same order in all the fuels.

3.2 Experimental methods

Bulk ash collection. Samples of fuel, new bed sand, bottom ash and fly ash (from ESP or baghouse) during all the measurement campaigns were collected and their elemental composition analysed. Special attention was given to fly ash and bottom ash analysis in processes B and C. Ash samples in amounts of kilograms were collected several times each day, and representative mixtures of the samples were analysed.

Fly ash sampling stations. Fly ash was characterised by aerosol measurement methods, downstream of the convective pass (before the ESP or baghouse) in all the processes. The flue gas temperature downstream of the convective pass is below 200 °C, which poses no specific problems for sampling. In addition, sample collections were also carried out in the convective pass (Process A), and upstream of the convective pass (Processes B and C), to observe the characteristics of the fly ash before vapour condensation and deposition on the heat exchanger surfaces took place.

Sampling methods for fly ash and inorganic vapours. Whenever feasible, the measurement instrument was located directly in the flue gas duct, and was allowed to heat up to the duct temperature prior to sampling. Otherwise, the flue gas sample was cooled by dilution, and withdrawn from the duct. Two kinds of systems for sample cooling and dilution were used. An axial dilution probe, using a principle presented by Biswas et al. (1989), was utilised at high temperatures upstream of the convective pass. The flue gas sample was aspirated through a tube (I.D. 10 mm, length 100 cm) made out of stainless steel. The walls of the tube were porous, and the cold dilution air was fed through the pores. The dilution air flow through the tube wall decreases sampling losses due

to thermophoretic particle deposition, diffusional particle deposition, and vapour condensation on the walls. The diluted sample gas was aspirated from the flue gas duct inside a stainless steel tube. The dilution probe was preceded by a cyclone collecting particles coarser than 3 μm, since transport of coarse particles through sampling lines would have resulted in severe sampling losses via gravitational settling and impaction.

Another dilution method was used downstream of the convective pass. It is based on ejector-type dilution units (Koch et al., 1988) preceded by a pre-cyclone. Here the sample is diluted with duct-temperature air in the first unit, and with room-temperature air in the second unit. The system was used for detecting sub-micron particles and for the collection of qualitative electron microscopy samples, i.e. in applications where the coarse particle sampling losses were not important.

Measurement and sample collection instruments.

Filter sampling system. In processes B and C, the condensed-phase ash and the vapour-phase species were detected separately upstream of the convective pass (flue gas temperature 800 - 850 °C). Particles were collected on a pre-cyclone and a quartz fiber filter. Vapours were condensed on the axial dilution probe and collected on a polycarbonate (Nuclepore) filter.

BLPI. Ash particle mass size distributions were measured using a system based on a Berner-type Low-Pressure Impactor (BLPI) preceded by a cyclone (Hillamo and Kauppinen, 1991; Kauppinen, 1992; Kauppinen and Pakkanen, 1990). In an impactor, the sample gas flow is directed through jets towards an impaction plate. The gas goes around the plate, but particles larger than the cut-diameter d_{50} are not able to follow the curved flow, but are impacted on the plate. BLPI has a good enough size resolution so that the fine and coarse ash particle modes formed during the combustion process can be observed separately. The system has been used previously by VTT in pulverised and fluidised bed coal combustion, as well as in kraft recovery boilers, to measure size distributions in flue gas downstream of the convective pass. In Process A, BLPI was implemented also in in-duct measurements at a flue gas temperature of 650 °C.

Analysis methods. The following elemental analysis methods were used for analysis of the bulk ash and fly ash particle samples; flame atomic absorption spectroscopy (FAAS), graphite furnace atomic absorption spectroscopy (GFAAS), inductively coupled plasma atomic emission spectroscopy (ICP-AES), inductively coupled plasma mass spectroscopy (ICP-MS), particle-induced X-ray emission (PIXE), and instrumental neutron activation analysis (INAA). Ion chromatography (IC) was used for detecting water-soluble ions.

Particle morphology was studied with a field-emission scanning electron microscope (FE-SEM, Leo DSM 982 Gemini). An acceleration voltage of 0.7–5 kV was used for imaging.

3.3 BLPI operation at 650 °C

One of the goals of this work was to study the suitability of an in-duct low-pressure impactor sampling technique for the ash particle mass and compositional size distribution measurements in the superheater section of a CFBC plant, at a temperature of 650 °C. Therefore, the method is discussed here in more detail. Materials used in collection substrates and gaskets had to be replaced for measurements at 650 °C. Polycarbonate substrates, greased to prevent bouncing of the impacting particles from the substrates, were replaced by ungreased stainless steel (AISI 316) substrates. The steel substrates were pre-heated at 700 °C for at least 60 hours before the measurements. The viton gaskets were replaced by graphite ones.

3.3.1 Operational parameters of the BLPI as functions of gas temperature

To determine the mass size distribution with an impactor, the operational parameters must be known in the measurement conditions. The gas temperature affects the gas flow rate through the impactor as well as the cut-diameters $d_{50,i}$ of each impactor stage i. The cut-diameter describes the collection characteristics of an impactor stage. According to the definition, stage i collects 50 % of the particles with diameter $d_{50,i}$.

The flow rate through an impactor with choked-flow stages (such as BLPI) remains constant during the measurement without any regulation, as long as the pressure downstream of the impactor remains low enough for the flow to be choked. During BLPI-measurements, the downstream pressure is set to 80 mbar. The gas mass flow rate Q of an impactor with choked-flow stages depends on the temperature T and on the inlet pressure P as

$$Q = Q_0 \frac{P}{P_0} \sqrt{\frac{T_0}{T}} \cdot C(T, T_0),$$

(25)

where Q_0 is the mass flow rate at T_0 and P_0 (Biswas and Flagan, 1984). $C(T,T_0)$ is a correction coefficient due to the temperature-dependence of the ratio of specific heats, but it has only a minor effect on the mass flow rate. C is equal to 0.98, when $T_0 = 20$ °C and $T = 650$ °C. The gas flow rate through the BLPI was measured in the laboratory at the inlet pressure of 1 bar and in the temperature range of 20–460 °C. The measured flow rate agreed with the theory within an accuracy of 5 %.

The eleven stages of the BLPI are numbered against the direction of flow, so that the sample flow first meets Stage 11 that collects the largest particles. Stage 1 collects the smallest particles. The d_{50} of the low-pressure Stages 1–6 have been experimentally determined at an inlet temperature of 20 °C, upstream pressure of 1.02 bar, and downstream pressure of 0.08 bar (Hillamo and Kauppinen, 1991). For the incompressible flow stages (7–11) the d_{50} are calculated using Marple's theory (Rader and Marple, 1985).

The d_{50} in conditions other than during calibration can be obtained by assuming that the Stokes number corresponding to d_{50} (Stk_{50}) remains unchanged (Hinds, 1999).

$$\text{Stk}_{50} = \frac{\rho_p d_{50}^2 V_j C_c}{9 \eta W},$$

$$C_c = 1 + \frac{\lambda}{d_{50}} \left(2.34 + 1.05 \cdot \exp\left(-0.39 \frac{d_{50}}{\lambda} \right) \right),$$

(26)

where the jet velocity V_j is calculated assuming adiabatic gas flow (Hering, 1987), C_c is the slip correction factor and W is the impactor stage jet diameter. λ is calculated from equation (7). In the super-micron size range, $C_c \approx 1$ and $\text{Stk}_{50} \propto \rho_p d_{50}{}^2$. At the other extreme of very small particles, C_c is approximately proportional to $1/d_{50}$, and Stk_{50} is correspondingly proportional to $\rho_p d_{50}$. For particles of any size, $\text{Stk}_{50} \propto d_{ae,50}{}^2$. Thus, impactor classifies particles according to their aerodynamic diameter.

The calculated $d_{ae,50}$ for each stage at the inlet temperatures of 160 °C and 650 °C are shown in Table 4 in Paper II. The d_{50} values of the incompressible stages are not sensitive to the temperature, whereas in the lowest stages the d_{50} values decrease significantly as the temperature increases. It would be possible to leave out Stage 1 during measurements at 650 °C, and still collect as small ($d_{ae} > 0.02$ μm) particles as at 160 °C with all the stages.

The assumption that Stk_{50} does not depend on temperature has been studied by Parker et al. (1981). They found no significant deviation from the theoretical predictions when a one-stage impactor was operated under incompressible flow conditions at temperatures up to 800 °C, using ceramic collection substrates. However, particle bouncing was found to be excessive, interfering with the data, when bare metal collection substrates were used to collect solid, hard-surfaced particles.

3.3.2 Analysis of samples collected on ungreased steel substrates

The samples were analysed gravimetrically by weighing the collection substrates before and after the sample collection, as well as chemically with ICP-MS, GFAAS, FAAS and IC methods. The two distinct fly ash modes, fine mode at $d_{ae} < 0.6$ μm and coarse mode in the size range of 1–100 μm, could be observed both gravimetrically and by chemical analysis (Figures 1,3 and 4 in Paper II). The fine mode was shown to consist of alkali sulphates, predominantly K_2SO_4 (50 mg/Nm^3). No condensed chlorides at concentrations above 0.01 mg/Nm^3 were present.

The ungreased steel collection substrates were found to cause some analytical problems. The ash collected on the substrates, especially at the upper stages ($d_{ae} > 1$ μm), was loosely attached to the substrates. This resulted in inaccuracy in

detecting the mass, as some of the ash was detached when the substrates were handled prior to weighing. The steel substrates were also found to gain mass, due to reactions with the flue gas, presumably by oxidation. The BLPI was usually preceded by a cyclone with a cut-diameter of 8 µm to prevent overloading of the upper stages. In the last one of the three samples collected at 650 °C, a smaller cyclone with a cut-diameter of 1.5 µm was used. In this sample, the coarse mode mass size distribution could be measured without being biased by the ash detachment and substrate reactions. The mass concentration in the size range of $d_{ae} > 1$ µm was 13 % lower in the last sample than in the other samples, suggesting that the experimental accuracy was also reasonable in the other samples (Table 6 in Paper II).

Bouncing of particles from the upper BLPI-stages may have taken place. However, the coarse mode particles ($d_{ae} > 1$ µm) did not end up in the sub-micron BLPI stages. This can be seen by the fact that Ca and Mg were observed only in the size range $d_{ae} > 1$ µm (Figure 3 in Paper II).

A challenging task was to find a suitable method for separating ash samples for chemical analysis. Our usual procedure is to cut one fourth of the substrate for analysis, but it was found to result in problems with steel substrates. The problems were due to ash detachment, especially when cutting the substrate, as well as due to the analytical problems caused by the oxidised steel matrix. The most successful sample separation method was to wipe the ash piles from the substrate with a clean paper tissue, which was then analysed.

3.3.3 Transformation of the sample aerosol inside the BLPI

Condensation and volatilisation. The temperature and pressure of the gas sampled through the BLPI remains unchanged until the low-pressure stages are reached. The decrease in pressure, and thus in the partial pressure of vapours, may cause volatilisation of the species having a concentration close to saturation. The flow at the impactor jets is assumed to be adiabatic, which results in aerodynamic cooling of the gas at the low-pressure stage jets (Biswas et al., 1987). Aerodynamic cooling may cause condensation of vapours, which is a contrary effect to pressure-decrease-initiated volatilisation.

The pressure drop in the BLPI is caused when the flow is forced through the jets located prior to the collection plate at each stage. The total jet area is small enough to result in significant pressure drops in Stages 1–5. The pressure downstream of the BLPI is always kept at 80 mbar while measurements are being made, and the inlet pressure is approximately 1 bar. The pressures between the stages, as calibrated at room temperature, are presented in Table 5 in Paper II. When the upstream and downstream pressures are fixed, the pressures between the stages do not depend particularly on the gas inlet temperature, even if the suction power needed to maintain the downstream pressure at 80 mbar does. Table 5 in Paper II also shows the temperatures in the jets at each stage. They were estimated assuming that the jet flow is adiabatic (no heat transfer from the metal), and that after the jets, the gas temperature is restored to the inlet temperature (due to heat transfer from the metal) before the next stage (Biswas and Flagan, 1984).

Condensation due to aerodynamic cooling may result in both the size and total mass concentration of particles collected in the low-pressure stages ($d_{ae} < 1$ µm) being over-large. After the sampling is finished, the pressure and temperature inside the impactor are increased back to the values prevailing at the impactor inlet. This may result in volatilisation of the excess mass. Pressure-decrease induced volatilisation, on the other hand, results in the size and total mass concentration of the particles being too small. The volatilised species are, of course, not recovered after the sampling is finished.

The ratio of partial vapour pressure at the ith stage, p_i, to that at the BLPI inlet, p_{inlet}, is the same as the ratio of the total gas pressure P,

$$\frac{p_i}{p_{inlet}} = \frac{P_i}{P_{inlet}} \ .$$
(27)

Volatilisation inside the BLPI may occur, if the p_i of the species of interest decreases below its saturation vapour pressure $p_s(T_{inlet})$. Here the saturation vapour pressure is the one at T_{inlet}, since it is assumed that the gas temperature is restored between the jets to the inlet temperature. Thus, volatilisation may occur at the ith stage if

$$p_{inlet} < \frac{P_{inlet}}{P_i} p_s(T_{inlet}) \,. \tag{28}$$

On the other hand, vapour condensation may occur at the ith stage if

$$p_{inlet} > \frac{P_{inlet}}{P_i} p_s(T_i) \,, \tag{29}$$

where T_i is the jet temperature of the ith stage. Condensation takes place on the aerosol particles and not on the collection substrate, because the substrate temperature is not decreased remarkably. For this reason, the condensed vapour may collect at a lower stage than where it was actually condensed.

The volatilisation and condensation rates inside the BLPI are difficult to estimate. However, the largest possible effect of their occurrence can be calculated assuming that an equilibrium condition is reached. Condensation and volatilisation of KCl inside the BLPI were of concern when in-duct measurements were made at 650 °C. The other species studied were condensed at clearly higher or lower temperatures, and were not sensitive to the conditions inside the impactor.

Figure 3 shows the maximum and minimum limits for the condensed-phase KCl inside the BLPI calculated using the equations (28) and (29). The mass concentration of condensed KCl at the BLPI inlet is also shown in Figure 3, assuming that condensation in the flue gas duct has reached equilibrium state, $p_{KCl} = p_{s,KCl}$. The KCl concentration corresponding to the saturation vapour pressure at 650 °C is 24 mg/Nm^3, thus the concentration of condensed KCl at equilibrium is m_c-24 mg/Nm^3 for $m_c > 24$ mg/Nm^3, and 0 otherwise. The mass concentrations observed at Stages 6–11 ($d_{ae} > 0.4$ µm) do not deviate from the ones prior to sampling. Stage 5 is still fairly reliable for observing KCl at 650 °C, but significant uncertainties may be associated with the stages 1–4 ($d_{ae} < 0.2$ µm). The condensation, or volatilisation, inside the BLPI is probably not as excessive as Figure 3 suggests, but proving this would require a more detailed analysis of aerosol behaviour inside the impactor than the one presented here.

In our measurements, KCl was not observed with the BLPI at 650 °C. If condensed KCl had existed, it should have been observed at least at Stage 5,

where more than 50 % of the K_2SO_4 was observed. Downstream of the convective pass the KCl–concentration was 5 mg/Nm^3. The absence of condensed KCl at 650 °C is understandable, because the concentration needed for KCl to condense at Stage 5 was at least 16 mg/Nm^3 (Figure 3).
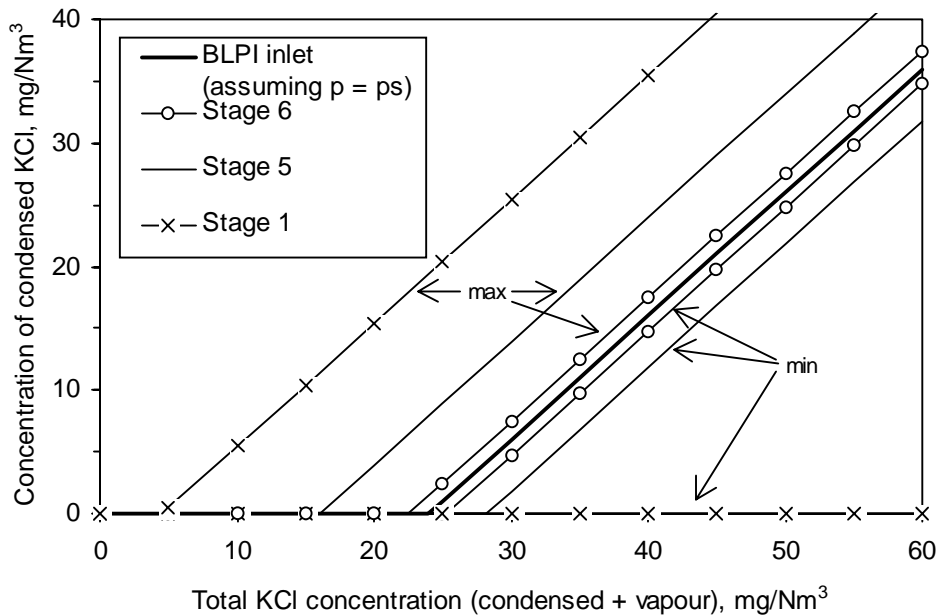
Figure 3. The concentration of condensed KCl inside the BLPI vs. total concentration. Maximum and minimum limits are shown. The inlet temperature is 650 °C. KCl is assumed to be in the equilibrium state at the inlet, $p = p_s$.

The lowest stages, where the condensation/volatilisation behaviour is the least known, could be omitted from BLPI at elevated temperatures. This is because the d_{ae} at the low-pressure stages are decreased when the temperature is increased. Only a small mass was collected at the two lowest stages at 650 °C (Figures 1, 3 and 4 in Paper II). If the lowest stages were not present, the pressure downstream of the BLPI would be higher. Accordingly, a less efficient pump would be needed and the requirements for gasket tightness would be less stringent.

Chemical reactions. Vapour species may become erroneously collected in the impactor if they chemically react with the collection substrate material, forming a condensed-phase compound. Particles collected on the substrate may also react with the flue gas during the measurement, or after the measurement but before the impactor is removed from the duct. The time for a reaction to take place is much longer for the collected particles (sampling times were 3–10 minutes) than for ash particles that penetrate through the convective pass in 1–2 seconds.

The reactions of interest in our case include reactions of i) gaseous HCl with the steel substrate and ii) gaseous SO_2 with previously collected alkali chloride particles. The reaction i) proceeds the oxidation of steel, but does not result in retention of Cl in the substrate, since the metal chlorides formed ($FeCl_2$ and $CrCl_2$) would be present in vapour form. The reaction ii) results in increases of K_2SO_4 and Na_2SO_4 in the samples, at the expense of KCl and NaCl.

In theory, it is possible that the 50 mg/Nm^3 of condensed K_2SO_4 observed at 650 °C originated partially, or completely, from condensed KCl via a chemical reaction with SO_2 at the substrate. The total KCl concentration of 66 mg/Nm^3 (42 mg/Nm^3 in condensed form and 24 mg/Nm^3 as vapour) would have been needed to introduce enough potassium for the formation of 50 mg/Nm^3 of K_2SO_4. The main argument against this hypothesis is the low amount of condensed phase Cl downstream of the convective pass (5 mg/Nm^3), compared to the 66 mg/Nm^3 required by the hypothesis. The KCl-concentrations upstream and downstream of the convective pass should be approximately the same, as will be shown in the section 4.4.2.

4. Results and discussion

4.1 Ash volatilisation from the fuel during the devolatilisation stage

The volatilisation of ash species from two types of wood chips was studied under O_2-free conditions with a laboratory-scale heated grid reactor (Paper I). The conditions simulate those during the devolatilisation stage of the fuel conversion process, when the hydrogen-rich volatile material is released from the fuel. The oxygen concentration on the surface of the fuel particle is minor at this stage, as the volatiles escaping from the fuel particle consume the oxygen available.

The wood chips had roughly the same overall ash concentration (1.3 % and 2.4 % of dry fuel) and potassium concentrations (0.2 %) as the fuels burned in the processes A–C during the pilot and power plant scale measurements (Table 3 in Paper I; Table 1). The most substantial difference in the fuel composition was in the concentration of Si. In the wood chips it was 0.2–0.5 %, which exceeds the Si concentration of the fuels in processes A–C (0.04–0.17 %), but was clearly lower than the 2.6 % of Si in the mixture of waste wood and paper mill sludge (Process D).

The fuel samples of about 100 mg each were distributed between stainless steel screens. The screens were heated, with a heating rate of about 800 °C/sec, to the final temperature of 850–950 °C. The holding time at the final temperature was 20 seconds. The screens were flushed with N_2, and the condensable matter (mainly tar) released with the N_2 was collected and analysed by the ICP-MS method. The sizes of the product particles were detected with BLPI. The particles were in the size range of $d_{ae} = 0.1–2$ µm. The small size of the particles indicates that the ash species present in the particles had been volatilised, instead of being fragments of ash or char particles carried away by the gas flow.

The analytical results show that the release of the alkali metals was minor. Less than 1 % of K and less than 5 % of Na was released from the fuel samples. The higher detection limit for Na, as compared to that of K, was mainly due to the lower concentration of Na in the fuels.

The results show that the release of alkali metals from the wood chip fuels studied here does not take place to a significant extent during the devolatilisation stage. If alkali vapour release occurs to a significant extent, it must take place during the char oxidation stage when O_2 is available at the fuel particle surface. The results obtained here for wood chips are in agreement with those by French and Milne (1994) and Dayton et al. (1995) for switchgrass. They found that the alkali vapour release took place predominantly during the char oxidation stage.

The released fractions of Ca, Si, Al and Mg were less than 4 %, which is expected due to their non-volatility. Si, together with the trace elements Pb and Zn, were the only elements whose released fractions significantly exceeded the concentrations detected during a background test. An empty screen, without a fuel sample, was heated in the background test. The background concentrations of Pb and Zn were at the most 26 % of the concentrations detected during the actual tests with the wood fuels. The released fraction of Pb, subtracting the background concentration, was 35 % from the whole tree chips and 75 % from the wood chips fuel fraction. The released fractions of Zn were 80 % and 56 %, respectively. Thus, Pb and Zn were released from the wood fuels to a much greater extent than K and Na, allthough the percentages given above for Pb and Zn are to be considered only as rough estimates due to the experimental inaccuracy involved.

4.2 Ash retention in the bed

The main motivation for studying ash attachment and reactions with the bed sand arises from ash-related problems in the combustion chamber (bed agglomeration) and in the ash recycling system (blocking in the cyclone and in the return leg from the cyclone to the bed). When ash behaviour in the convective pass is of concern, it is useful to know the characteristics of the ash entering the convective pass. The ash removed from the furnace with bottom ash represents the fraction of incoming ash that does not enter the convective pass.

Ash retention in the bed was studied most comprehensively during measurements in Process C (Paper IV). The ash flow rates to the furnace (fuel feed and sand feed) and from the furnace (bottom ash and fly ash) were

estimated and their chemical composition analysed. The mass balances of the total ash and inorganic elements were calculated from the data.

4.2.1 On the accuracy of the mass balance calculations

The mass balance evaluation involves several sources of inaccuracy, which are difficult to quantify. These are related to the steadiness of the process, accuracy of the mass flow rate values that are based on process data monitored at the plant, and on collecting a representative fly ash sample.

The unsteady process conditions cause inaccuracy in the mass balance mainly because of different response times of ash flows to changes in process conditions. Fly ash concentration reacts quickly (as demonstrated, for instance, in Figure 10 of Paper III), whereas the composition of the bottom ash shifts slowly with time. This is due to the large inventory of bed material compared to the feeding of ash-forming constituents into the furnace (for instance, of the order of 10 tons of bed material vs. 110 kg/hour of fuel-originated ash-forming constituents in Process C). The bed-material feed and removal rates may vary remarkably from day-to-day, according to the assessments by the power plant operating staff. However, the elemental concentrations in the bed material do not vary accordingly, since only a fraction of the total inventory in the bed is changed in a day.

The fly ash samples were collected upstream of the convective pass by a filter sampling system. Aerosol particles larger than about 10 µm have a tendency to distribute non-uniformly throughout the cross-section of the duct, after a bend or an obstacle. Representative sampling requires that the sample is collected at least 5–10 duct diameters away from the previous bend or obstacle in the duct (Hinds, 1999), but this kind of long straight part does not exist in the duct upstream of the superheaters. The sampling should also be carried out isokinetically, that is the sample nozzle orientation and diameter should be such that the flue gas flow entering the nozzle is not curved. Sampling was carried out by directing the nozzle towards the mean direction of flow, and by choosing the nozzle diameter so that the velocity in the nozzle was approximately the same as the mean velocity of the duct flow. This does not assure isokinetic sampling, as the flue gas flow direction and velocity fluctuate due to the highly turbulent nature of the

power plant duct flows. However, according to Hinds (1999), the anisokineticity caused by flow turbulence does not usually result in severe sampling errors.

To minimise the effect of the non-quantifiable inaccuracy sources, the fraction of element X retained in the bed, $BF(X)$, was calculated relative to that of Ca, $BF(Ca)$. The calculations were carried out for the amount of ash coming out from the furnace, $BF_{out}(X) / BF_{out}(Ca)$ (equation 5 of Paper IV) and for the amount of ash-forming constituents fed into the furnace, $BF_{in}(X) / BF_{in}(Ca)$, (equation 6 of Paper IV).

The fluctuating bottom ash removal rate Q_b and the fly ash mass flow rate Q_{fl} have only minor effects on the value of $BF_{out}(X) / BF_{out}(Ca)$, and are completely absent when $BF_{in}(X) / BF_{in}(Ca)$ is calculated. Otherwise, values for $BF(X) / BF(Ca)$ depend only on elemental concentrations that are less fluctuating than the mass flow rates. The possibly unrepresentative fly ash sampling affects only $BF_{out}(X) / BF_{out}(Ca)$.

The mass balance is perfect if $BF_{out}(X) / BF_{out}(Ca)$ is equal to $BF_{in}(X) / BF_{in}(Ca)$, that is the calculated amount of X entering the combustion chamber equals to the amount of X removed with bottom ash and fly ash. Both of these values are shown for Process C in Table 2. Differences between the two values are not caused only by the experimental inaccuracy. The input of ash in the combustion chamber may differ from the output, as the mass of the solid material in the bed is not constant when a short period, such as two days, is considered.

4.2.2 Results

Non-volatilised species, e.g., Ca, P and Mg, become retained via ash particle collision and attachment to sand particles. The probability that an ash particle is retained on the sand particle after a collision depends on the ash particle size and surface properties. This results in different values of $BF(X)$ for species that are present in ash particles of different size and composition. A species that reacts with quartz is retained with increased efficiency, as the reaction product avoids the disintegration of ash particles from the sand via bed attrition. P and Mg were, in most cases, retained with a lower efficiency than Ca (Table 2). This may be associated with the finding by Latva-Somppi et al. (1998a), that quartz

had reacted with Ca, and the deposit layer on the sand particles was enriched with Ca-rich particles of about 1 μm in size.

Table 2. The fraction of each element X retained in the bottom ash [BF(X)] relative to that of Ca [BF(Ca)] calculated using equation 5 and 6 in paper IV.

	Willow and Wood pellets	Willow (day), Forest residue (night)	Forest residue		Paper mill sludge and waste wood
Process	A	B	C		D
BF(Ca)	n.a.	0.4	0.41	0.31	0.05–0.1
	$BF_{in}(X)/$ $BF_{in}(Ca)$	$BF_{in}(X)/$ $BF_{in}(Ca)$	$BF_{out}(X)/$ $BF_{out}(Ca)$	$BF_{in}(X)/$ $BF_{in}(Ca)$	$BF_{out}(X)/$ $BF_{out}(Ca)$
Ca	1	1	1	1	1
P	0.62	0.58	0.76	1.00	1.08
Mg	1.08	0.87 [a]	1.00	1.06	0.54
K	1.18	1.12	1.39	1.44	0.43
K excl.[b]	1.28	1.28	1.50	1.57	0.43
S (incl. SO_2)	0.62	0.11	0.13	0.17	n.a.
Cl	< 0.01	< 0.04	< 0.3	< 0.05	n.a.
Zn	1.72 [c]	1.49	1.83	1.40	1.37
Pb	< 0.03	0.54	0.67	0.69	0.2
Cd	< 0.2	0.02	0.04	0.03	< 0.5

[a]) Fly ash concentration based on ESP-collected ash.
[b]) Excluding the volatilised K that ended up in fine mode fly ash particles.
[c]) Assuming sand was Zn-free.

Species that are gaseous at the bed temperature cannot be retained in the bed unless they chemically react, forming non-gaseous compounds. Chlorine formed only gaseous compounds, as no Cl was found in the bottom ash. Also S, Pb and Cd were depleted in the bottom ash more clearly than any of the non-volatile elements, indicating their partial release as gaseous species from the combustion chamber. Potassium was retained in the bottom ash with higher efficiency than Ca during Processes A–C despite the fact that some of the potassium escaped the furnace as KOH and KCl vapours (Table 2). The high value of *BF(K) / BF(Ca)* can be explained by a reaction of potassium with quartz, forming potassium

silicates, observed by Latva-Somppi et al. (1998a). The reaction of potassium with quartz may take place via:

i) Diffusion of vapour molecules (KOH, KCl and/or K_2SO_4) to the surface of bed material particles, followed by a surface reaction (also condensation in the case of K_2SO_4).

ii) Deposition of sub-micron K_2SO_4 particles on the bed material, followed by a reaction. Sulphur released from the K_2SO_4 + SiO_2 -reaction may become volatilised as SO_2. KOH and KCl are not present in the particle-phase at the bed temperature.

iii) Deposition of super-micron particles on the bed material, followed by a reaction of potassium present in the super-micron particles with quartz. This mechanism may result in enrichment of K in the bottom ash relative to Ca in the case where super-micron particles are detached from the bed particle after potassium has reacted with quartz.

Since a considerable fraction of K reacts with quartz sand, it is presumable that K also reacts to a significant extent with the Si originating from the fuel. How does the Si-content of the fuel affect the behaviour of potassium? The amount of quartz sand bed material in the combustion chamber exceeds that of the ash-bound quartz and silicates, due to the long residence time of sand as compared to ash. However, the Si in ash is able to bind a larger fraction of alkali metals than would be expected from just considering the relative quantities of ash-based Si and sand-based Si. Firstly, fuel-originating Si, unlike the bed sand, is originally present in the same fuel particles as the alkali metals. Secondly, the number of vapour molecules colliding with a group of monodisperse particles with a given total mass, is proportional to $1/d^2$ (Hinds, 1999). This is in favour of vapour molecule collisions with ash particles instead of sand particles, since the ash particles are smaller (up to tens of μm) than the bed sand particles (hundreds of μm).

Most of the Si fed into the combustion chamber originated from the fuel in Process D, unlike in the case of B and C (Table 3). *BF(K) / BF(Ca)* was, indeed, significantly lower in Process D compared to the other processes (0.43 vs. 1.12– 1.4, Table 2). The difference is even clearer, when the potassium that is known

not to have reacted with Si (K found in the fine mode fly ash particles) is not considered (0.43 vs. 1.3–1.6, Table 2).

Table 3. Si fed into furnace as quartz sand and in fuel.

	Process	Si from fuel, tons/day	Si from sand, tons/day	Si from fuel / Si from sand
Willow (day), forest residue (night)	B	0.04–0.2	0.4	0.1–0.5
Forest residue	C	0.22	3.1	0.07
Sludge + waste wood	D	3.5	0.5–1	3.5–7

The original presence of K in a more effectively depositing ash-particle fraction compared to Ca would be an alternative explanation for the fact that *BF(K) / BF(Ca)* > 1 in Processes A–C. However, it is contradictory to the finding that *BF(K) / BF(Ca)* < 1 in Process D, and is thus not a satisfactory explanation.

Zinc was enriched in the bottom ash also in Process D, unlike potassium. The data presented in Section 4.1 show that Zn preferably becomes volatilised from the fuel during the devolatilisation stage, instead of reacting with quartz and silicates (at least from the wood chips used in the experiments described in the paper I). On the other hand, Dahl and Obernberger (1998) have shown that Zn in the fly ash, formed in Process C was not volatile, neither in air nor in an O_2-free atmosphere. The absence of Zn in the fine mode fly ash particles (Papers III and VI) also indicate that the volatile Zn chemically reacted with the ash and formed non-volatile compounds.

The different behaviour of Zn, when compared to that of K, in Process D can be explained in the following way. Zn is volatilised to a great extent during the devolatilisation stage, whereas a major fraction of K is not volatilised but reacts with the fuel-originated quartz and silicates without volatilisation. This results in *BF(Zn) / BF(K)* > 1 in all the processes, even if the volatilised fractions of K and Zn may have been distributed similarly between the quartz sand and the fuel-originated silicates.

The data presented for the different elements show that a sufficient estimate of bed-retention fraction for a given species cannot be based only on information about its volatility. The chemical reactions with the quartz were found to be important contributors to bed retention. Also, the data for Zn indicate that the absence of a species in the fine fly ash particles is not convincing evidence of its non-volatility. This situation should also be considered with regard to the alkali metals.

4.2.3 Input from the sand to fly ash

The sand-originated species may end up in the fly ash via i) fragmentation of sand particles to a size small enough to avoid recycling by the process cyclone, or ii) by volatilisation. The Si-concentration in fly ash was clearly higher than in the laboratory-prepared ash during combustion of willow, in Process A (3.8 % vs. 5–7 %) and especially in Process B (2.1 % vs. 9.5 % in daytime). In order to transfer Si from bed sand to fly ash, the sand particles have to be fragmented into a size small enough to avoid recycling by the process cyclone. A quartz transformation to silicates via reactions with potassium compounds has been proposed to promote fragmentation (Latva-Somppi et al., 1998a). In the case of Process B, the high Si concentration in fly ash during the daytime may have come from the forest-residue-originated ash being attached onto the bed material during the night, and released again during the daytime.

Table 4 shows the fraction of the ash-forming constituents, including contributions from both the fuel and the sand, ending up in the fly ash. An interesting result concerning alkali metals can be observed. The percentage of K ending up in the fly ash was approximately the same as that of Na, despite the fact that the origin of these two elements was clearly different in Process C.

The majority of K was fed with fuel, whereas for Na, input with sand was dominant. In the combustion chamber, K and Na were settled in a state where their division between fly- and bottom ash was approximately the same, about one quarter in fly ash in Processes B and C. More than half of the fuel-originated K reacted with the bed sand in Process C. On the other hand, no significant net transfer of sodium between the fuel and the bed material took place, as the fuel already contained about one quarter of Na to start with.

Table 4. The percentage of ash-forming species originating from the fuel, and the fraction of the total input (fuel + sand) that ended up in the fly ash. The limits given for percentages originating from the fuel in Process B vary from 100 % willow to 100 % forest residue.

	Willow (day), forest residue (night) (B)		Forest residue (C)		Sludge and waste wood (D)	
	From fuel, %	To fly ash, %	From fuel, %	To fly ash, %	From fuel, %	To fly ash, %
K	89–93	35	65–68	26	> 99	96–99
Na	48–70	29	26–29	22	96	92–98
Ca	> 99	47	98	57	100.00	92–98
Si	8–31	10	9	5	91	89–97
P	> 99	69	97–98	67	n.a.	97–99
S	> 99	94	98	93	n.a.	94–98

4.3 Characteristics of the fly ash entering the convective pass

Characterisation of the vapours and fly ash that enter the convective pass is useful when the ash particle deposition and vapour behaviour in the convective pass is studied. The data of interest include concentrations of the fly ash and inorganic vapours, as well as the size distribution and morphology of the ash particles. This paragraph is mainly based on data from the high-temperature measurements upstream of, or in, the convective pass. The results from the measurements downstream of the convective back pass are discussed only inso much as the alteration in the convective back pass is not, according to our understanding, important.

4.3.1 Characterisation of fly ash upstream of the convective pass

In the following, the state of the ash-forming constituents (vapours, fine particles and coarse particles) upstream of the convective pass are discussed briefly. The alteration of the aerosol in the sampling has to be considered while interpreting the data. For this reason, the interpretation is not based on one measurement

technique only, but on a combination of results from the different sampling methods.

Inorganic gases and vapours. The concentration of SO_2 in-duct was of the order of 10 ppm in the processes that we studied. The low SO_2-concentration, when compared to combustion of most coals, is mainly due to the low amount of sulphur in wood. Also, a substantial conversion of SO_2 into condensed form takes place, even if a sorbent, e.g. limestone, is not utilised. Wood contains high amounts of Ca and K that react with SO_2 forming condensable sulphates. In Processes B and C, 50 % and 20 % of S were present as SO_2, respectively.

Apart from SO_2, alkali chlorides were the most significant ash-forming constituents that were found in the gas phase at 800 °C (Processes B and C) and at 650 °C (Process A). In Process A, condensed K_2CO_3 was present in fine particles at 160 °C but not at 650 °C, indicating that the corresponding amount of potassium must have been in vapour-phase at 650 °C.

According to mass balance calculations, most of the Cl was present in non-condensable form (presumably as HCl) in Processes B and C.

Fine fly ash particles. The fine mode particles in the size range $d_{ae} < 1$ µm are formed via homogenous nucleation of vapours. Alkali sulphates were the only compounds significantly present in sub-micron particles already upstream of the convective pass. The fine mode mass concentration upstream of the convective pass was clearly higher in the combustion of willow (Processes A and B) compared to the other processes (Figure 4; Figure 6 in Paper III). This is due to the large amount of alkali sulphates formed from willow.

The presence of alkali sulphates in condensed form at 650 °C was directly observed in Process A. In Processes B and C, alkali sulphates were collected by a quartz fiber filter at about 800 °C. This is, however, not convincing evidence that alkali sulphates were predominantly condensed at 800 °C. Gaseous, supersaturated alkali sulphate molecules may have become trapped on the filter by condensation. More convincing evidence can be found by comparing the fine particle size distributions upstream and downstream of the convective pass. In Process C, the fine particles were dominated by the alkali chlorides. Here the size and number concentrations of the fine mode particles were different at the

different sampling stations (Figure 4 in Paper IV). This indicates that the condensation took place at different times, that is after sampling upstream of the convective pass. On the other hand, the size and number concentrations of the fine particles in Process B, dominated by alkali sulphates, were similar, within the experimental accuracy (Lind et al., 1997). This suggests that the condensation of alkali sulphates took place before the sampling station upstream of the convective pass.
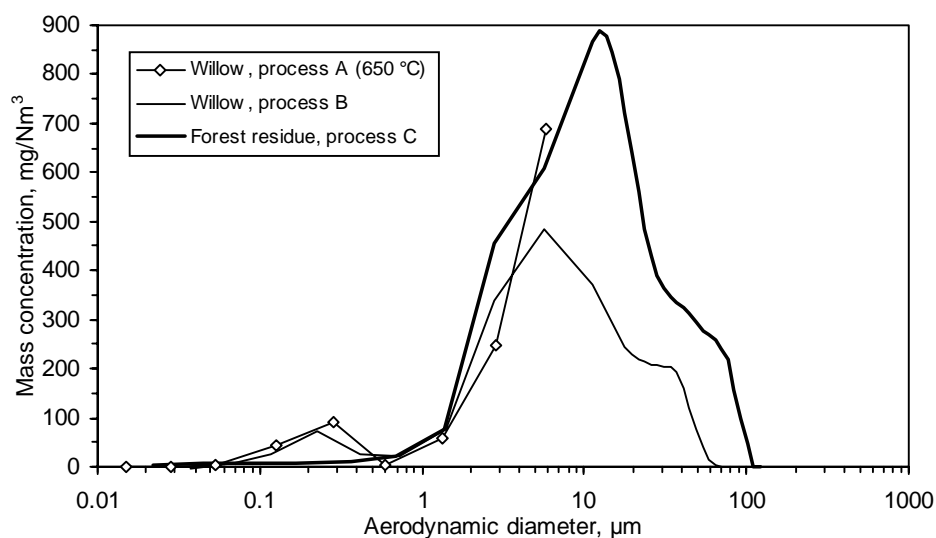

Figure 4. Fly ash mass size distributions upstream of the convective pass (processes B and C) and in the convective pass at flue gas temperature 650 °C (Process A, particles with $d_{ae} > 8 \mu m$ are not shown). The contribution of alkali chloride vapour condensed on the particles inside the sampling system has been extracted from the data concerning processes B and C.

There may have been sub-micron particles formed from volatilised refractory species already present prior to alkali sulphate condensation. The BLPI-samples in Processes A–C show minor concentrations of calcium in sub-micron particles. However, the concentrations are so small that it is not possible to conclude whether this indicates the existence of these elements in the fine ash particles, or merely coarse particle bouncing from the super-micron BLPI-stages.

The number concentration of the alkali sulphate particles upstream of the convective pass was not measured in any of the processes. However, the number concentration N (particles / Ncm^3) can be estimated from the mass size distribution measured in Process A with BLPI at 650 °C (prior to condensation of alkali chlorides),

$$N = \sum_i \frac{m_i}{M_i} = \sum_i \frac{6m_i}{\pi\rho_p d_i^3},$$
$$d_i = \sqrt{d_{50,i} \cdot d_{50,i+1}},$$

(30)

where summation is over all the BLPI-stages i (although only the 5 stages collecting the smallest particles contribute significantly), m_i is the mass concentration of the particles collected at the ith stage (based on the IC-analysis results), M_i is the mass of an individual particle collected at the ith stage, $\rho_p = 2.7$ g/cm^3 for K_2SO_4 and Na_2SO_4, and d_i is the geometric mean diameter of the particles collected at the ith stage. The cut-diameters $d_{50,i}$ are calculated using equation (26).

The estimated number concentration N was $3 \cdot 10^8$ particles / Ncm^3, excluding the particles in the 2 smallest stages, $d < 0.014$ μm, where the experimental inaccuracy is too large for a reliable estimate (Figure 5). The inaccuracy of N is greater the smaller d is. This is due to the fact that the contribution of the inaccuracy in m_i to the inaccuracy in N is proportional to $1/d_i^3$ (equation 30). It is possible that the number of particles formed by nucleation was considerably higher than the detected $\approx 10^8$–10^9 particles/cm^3, and it decreased to the detected level through coagulation. Coagulation limits the number concentration down to 10^8–10^9 particles/cm^3 in the order of 0.1–1 seconds, no matter how high the original concentration is (Section 2.4).

Coarse fly ash particles. The coarse mode in the super-micron size range contributed over 90 % of the fly ash mass upstream of the convective pass in the processes studied. Coarse mode fly ash contains the ash-forming species fed into the combustion chamber, with the exception of the species ending up in the bottom ash as well as volatilised species ending up in the fine ash particles (alkali chlorides and sulphates).
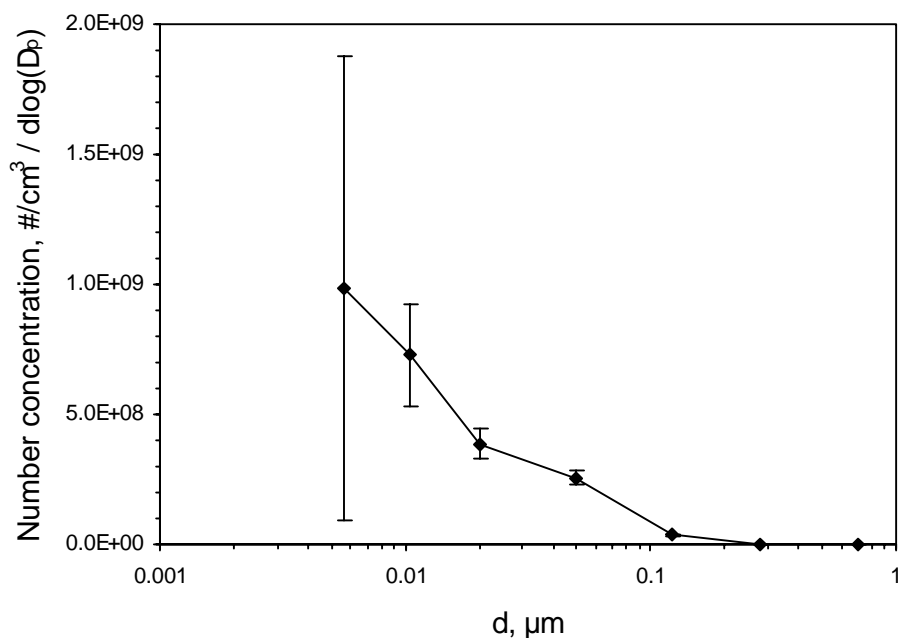
Figure 5. Number size distribution of fly ash particles at 650 °C in Process A calculated from the mass size distribution data. Error bars are calculated assuming a background of 200 μg/Nm^3 at each stage + a relative error of 10 % in the observed mass concentration.

The concentrations of Ca and P in the laboratory-prepared ash were found to be reasonable estimates for their concentrations in the coarse fly ash particles (Table 5). These non-volatile species do not end up in the fine ash to a significant extent. The differences in the bed-retention fractions were not large enough to cause significant enrichment or depletion of Ca and P in the coarse fly ash.

The concentration of sulphur in the coarse particles can be either remarkably higher or lower than in the fuel. S is retained in the bed to a lesser extent than ash-forming constituents in average. This results in enrichment of S in the convective pass (fly ash + SO_2). In Process C, 80 % of sulphur ended up in the coarse fly ash particles, resulting in concentration of S in coarse fly ash more than twice that in laboratory-prepared ash (Table 5). This is apparently due to reactions between SO_2 and CaO resulting in formation of $CaSO_4$. Anhydride was

observed in coarse particles by XRD, as mentioned in Paper VI. Gaseous SO_2 contributed the remaining 20 % of S. In Process B, the formation of $CaSO_4$ was less significant. Only about one quarter of S was present in the coarse particles, resulting in depletion of S in coarse fly ash. Another quarter was found as alkali sulphates in the fine particles, and one half remained as SO_2. The Si-concentration can be larger in the fly ash when compared to the laboratory-prepared ash due to release of bed sand. This was the case with the willow combustion processes, A and B.

Table 5. Concentration of ash-forming constituents in the laboratory-prepared ash (Lab) and in the coarse fly ash upstream of the convective pass (CFA).

	Willow + wood pellets (Process A)		Willow (Process B)		Forest residue (Process C)	
	Lab (%)	CFA (%)	Lab (%)	CFA (%)	Lab (%)	CFA (%)
Ca	25.8	22 [a]	21.2	21.1	20.8	20.2
Si	3.8	7 [b]	2.1	9.3 [c]	8.3	7.5
P	3.8	4.4 [b]	4.8	5.0	2.2	2.8
K	12.9	6.5 [a]	14.3	6.1	7.1	3.6
Na	0.4	n.a.	0.4	0.6	0.8	1.0
S	3 [d]	n.a.	2 [d]	0.9	2 [d]	4.9
Cl	1 [d]	n.a.	0.6 [d]	0.2	1.2 [d]	0.3

[a]) In the convective pass, at 650 °C.
[b]) ESP-collected ash (downstream of the convective pass).
[c]) Forest residue burned at night (8.3 % Si in the laboratory-prepared ash) may have contributed to the amount of Si released from the bed sand to fly ash.
[d]) Concentration of S or Cl in fuel divided by ash concentration in fuel. S and Cl were analysed from non-ashed fuel samples.

The coarse fly ash particles were found to have a very irregular surface structure in all the processes studied (Figure 6). The most common coarse particle structure was an agglomerate of hundreds of sub-micron primary particles. The combustion temperature has not been high enough for coalescence of ash particles into compact spheres. Some spherical coarse particles were observed only in Process D, where the fuel included also sludge. The particles were heterogeneous in chemical composition. The specific surface area of the coarse fly ash particles was 7–10 m^2/g, as determined by a nitrogen absorption method
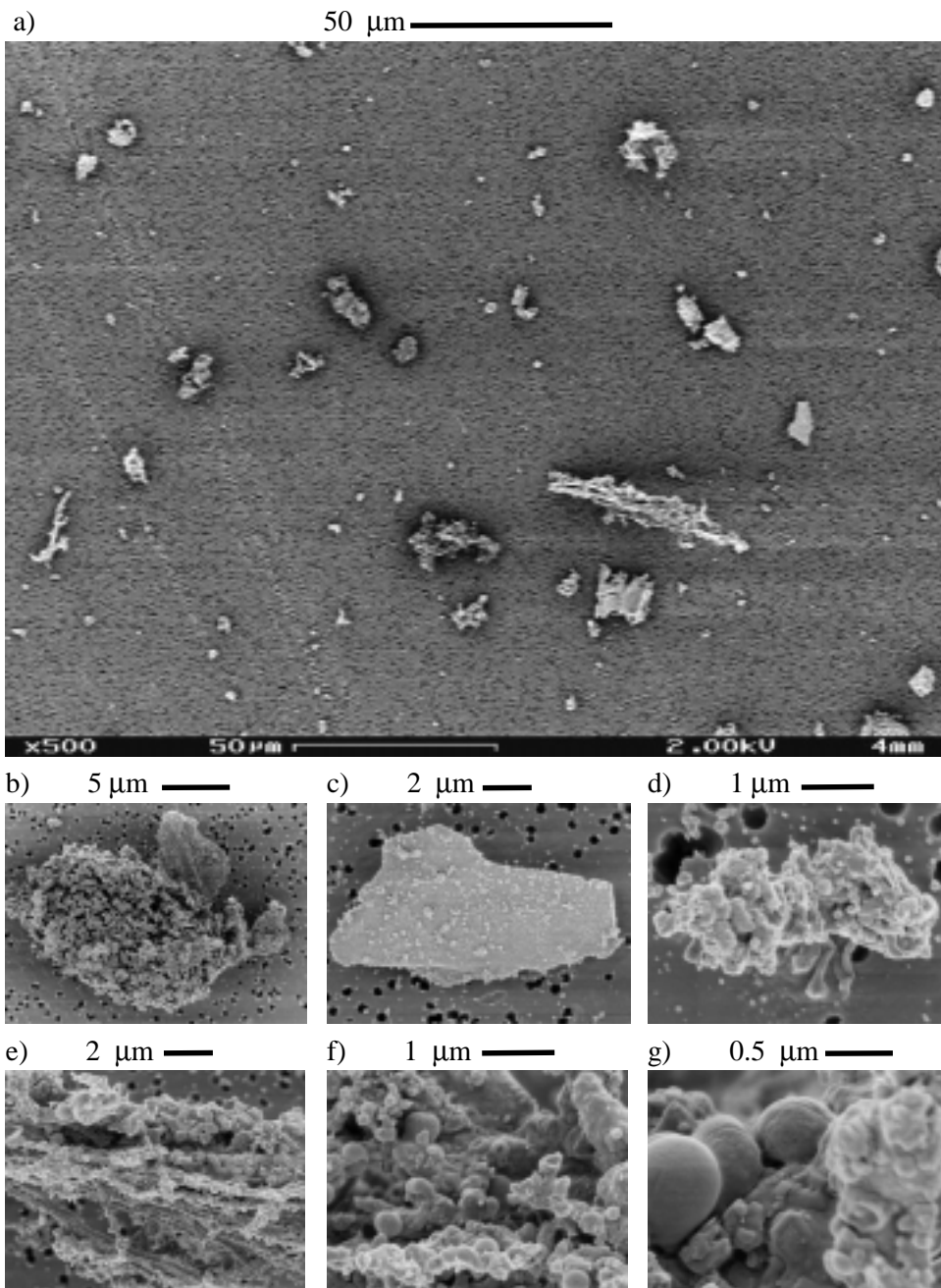
Figure 6. SEM-micrographs of coarse fly ash particles formed during combustion of willow + wood pellets (Process A). Figures e)-g) show enlargement of the coarsest (50 µm long) of the particles shown in a).

(Lind, 1999; Papers III and VI). The surface area is similar to that of spherical particles with $\delta \times d = 0.7–0.9$ g/m^2, or $d = 0.3–0.4$ μm for particles with a typical fly ash-density ($\delta = 2.5$ g/cm^3). The surface area of spherical particles with $d = 3$ μm would be 0.8 m^2/g, that is an order of magnitude lower than the observed one. The particle shape has an effect on vapour condensation on, and reaction with, coarse particles, as pointed out in Paper VI and by Lind (1999). The effect of particle shape is discussed briefly in Sections 4.4.3 and 4.5.

4.3.2 The effect of fuel composition on the extent of K$_2$SO$_4$ and KCl formation

Alkali silicates are present in the coarse fly ash particles, since quartz and silicates are not volatilised appreciably. On the other hand, alkali sulphates and chlorides are formed mainly via vapour – vapour reactions and are enriched in the fine particles. The fraction of Na in the sub-micrometer ash particles has been found to decrease with the increasing Si content in the fuel in the pulverised combustion of bituminous coals and lignite at 1480 °C (Neville and Sarofim, 1985). The high concentration of silicates facilitates the reaction of K and Na with them. In fact, the amount of gas-phase alkali compounds formed in combustion of straw was found to be reduced when straw was co-fired with coal. This was probably due to the capture of straw-originated alkali by the clay minerals in the coal (Dayton et al., 1999a). Also, the Si concentration in the fuel often correlates with the fraction of alkali metals present originally as silicates in the fuel. In pulverised coal combustion, sodium silicates are formed most effectively in the temperature range of 1000–1300 °C from the alkalis that are present in non-chloride form (Wibberley and Wall, 1982a and 1982b; Erickson et al., 1992). At lower temperatures, alkali diffusion into silica structure probably limits the reaction rate. Below 1000–1100 °C, the presence of sulphur in the combustion gas reduces alkali silicate formation, as alkali sulphate formation becomes more favourable. In FBC, the bed temperature (800 °C) is relatively low for efficient alkali silicate formation. In wood fuels, the concentration of non-chloride potassium is typically higher and the concentration of sulphur lower than in coals, which should favour alkali silicate formation.

The effect of fuel composition on the formation of fine potassium fly ash is studied in Figure 7. The parameters related to fuel composition include Si-

concentration, the amount of K that can be bound to sulphates and chlorides by the Cl and S present in fuel ($1.1 \cdot S + 2.44 \cdot Cl$), and the ratio of the two parameters described above. The processes presented include the processes studied in this thesis, CFBC of coal (Lind et al., 1994) as well as two bubbling fluidised bed combustion processes with sludge and biomass (Paper III; Latva-Somppi et al., 1998b). The variable on the y-axis is the fraction of fine mode K out of the total amount of K in the fly ash downstream of the convective pass. This variable is assumed to have a clear correlation with the variable of interest, which is the fraction of potassium as chloride and sulphate of all the potassium in the fly ash. The correlation is not perfect, since the ash retained in the convective pass is not considered, and some of the chlorides and sulphates are present in the coarse-mode particles.

There was only a minor concentration of alkali sulphates and chlorides during CFB combustion of bituminous coal (Lind et al., 1994). More than 99 % of the K and Na in fly ash were insoluble in water, probably present as silicates, even if only 74 % of Na and 97 % of K in the fuel were insoluble in water. Non-silicate sodium compounds reacted effectively with the quartz and silicates during the combustion process. Figure 7.a shows that the decrease in Si-concentration relative to the concentration of K in fuel resulted in an increase in fine potassium particle formation. This was the case with biomass alone as well as with the co-combustion of sludge and biomass. The concentrations of S and Cl in fuel, and their concentrations relative to that of Si, did not correlate with the potassium fine particle formation (Figure 7.b and c).

During CFB co-combustion of sludge and waste wood, the sludge feed was turned off for a short period of time, and the waste wood was burned alone (Figure 6 in Paper III). The number of ultrafine (< 0.1 µm) particles was slightly increased, even if the concentration in the coarser size range monitored (< 0.5–5 µm) was decreased by 30–50 % due to smaller ash concentration in waste wood compared to that in sludge. Increased ultrafine particle formation with waste wood alone was in agreement with the lower Si/(K + Na) -ratio in waste wood (8.2) compared to that in the fuel mixture during co-combustion (10.5). A similar test was carried out during BFB combustion of sludge and bark, described in Paper III. Now the difference in Si/(K + Na) -ratio was greater than during CFB (12.7 during co-combustion and 4.7 in bark). The increase in the ultrafine particle concentration was now more significant than during CFB

(Figure 11 in Paper III). However, a natural gas burner was used when the sludge was not fed, which may have affected the results.

a)

b)

c)
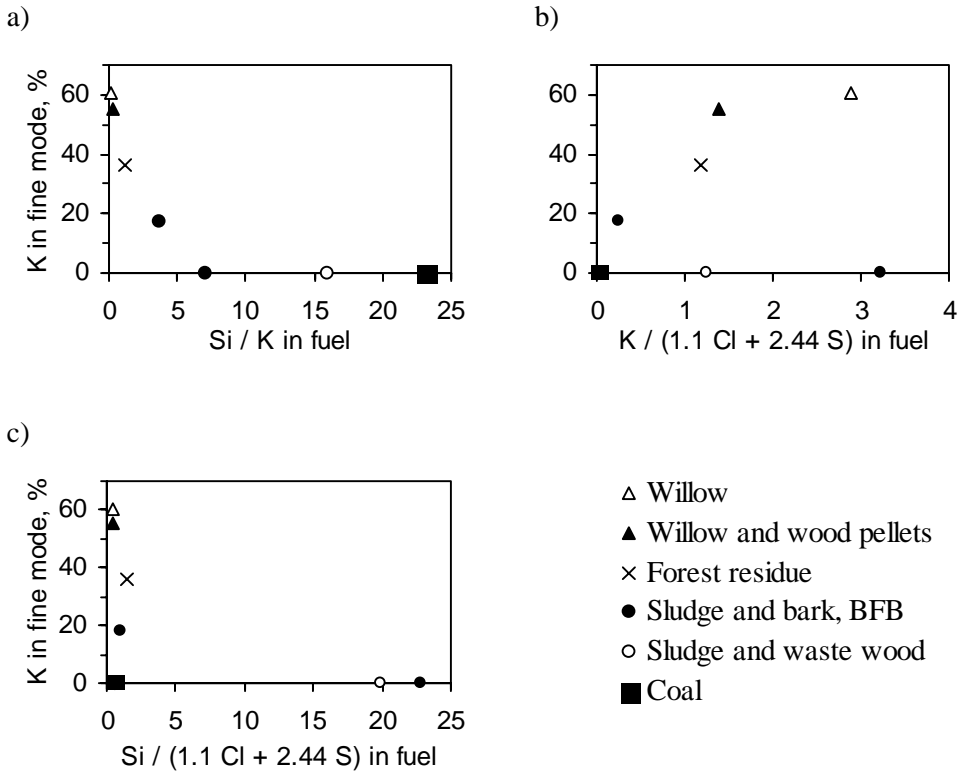
Figure 7. K in fine mode particles (KCl and K_2SO_4) of the total K downstream of the convective pass as a function of parameters describing fuel composition. Data is taken from Papers II, III, V, Lind et al. (1994) and Latva-Somppi et al. (1998b).

All of the processes took place with roughly similar combustion temperature (about 800 °C) and fuel moisture (about 50 %). When processes with greatly different conditions are compared, the fine particle formation can not be explained merely by the fuel Si/K ratio. For instance, during the laboratory-scale experiments reported by Latva-Somppi et al. (1998b), 4 % of K and 3 % of Na were in the fine mode particles when wet sludge was burned at 800 °C. When the same sludge was dried and burned at 880 °C, the fine ash fractions of K and Na were 33 % and 22 % respectively.

4.4 Ash deposition on the heat exchangers

The ash deposition efficiency on the heat exchanger surfaces in the convective pass was studied in Processes A–C. The fly ash size distributions upstream of the convective pass (Processes B and C), or in the convective pass at 650 °C (Process A) were compared to those downstream of the convective pass.

4.4.1 Mass concentration decrease in the convective pass

The most comprehensive studies were carried out in Process C. The accumulation rate of fly ash in the ESP was only 24–35 % of the rate of fly ash entering the convective pass, calculated by extracting the fuel-originated contribution of the bottom ash flow from the fuel feed flow. This is in agreement with the result that 70 ± 10 % of the ash was found to be deposited when the fly ash concentrations downstream and upstream of the convective pass were compared.

The first ESP ash sample was collected partially during a soot-blowing. As much as 2640 kg of fly ash was collected during this 3-hour sample that included the latter hour of the 2-hour soot-blowing. The fly ash accumulation rate in the convective pass must have been at least 55 kg/h to produce the 2640 kg or more that was released during the soot-blowing. The rate of fly ash collected by the ESP was 19 kg/h later that day, when soot-blowing was not being carried out. This rough estimate confirms that most of the fly ash must have been deposited in the convective pass when soot-blowing was not being carried out.

Results from the other processes also indicate that a majority of the fly ash is deposited in the convective pass (Table 6). The deposition efficiency was 60 ± 4 % in Process B (Lind et al., 1997). The decrease in mass concentration between the sampling stations at 650 °C and 160 °C in Process A was about 40 %. A reasonable estimate concerning Process D can be made from the bulk ash flow rate data, since the bottom ash fraction of the fuel-originated ash was only 5–10 %. The amount of ash-forming constituents fed into the furnace with the fuel corresponded to a fly ash mass concentration of 20 g/Nm^3. The concentration measured downstream of the convective pass was only 8 g/Nm^3, resulting in a deposition efficiency of about 60 %. The deposition efficiencies in coal combustion are typically much lower than the values obtained here for wood

combustion. For instance, during pulverised combustion of Polish coal, the fly ash mass concentrations measured after the convective pass were, on average, only 24 % (tests carried out in 1991) and 14 % (tests carried out in 1992) lower than the input to the combustion chamber calculated from the process data (Joutsensaari et al., 1994).

Table 6. Fly ash deposition efficiency in the convective pass when soot-blowing was not carried out.

	Process A	Process B	Process C	Process D
Deposition efficiency	> 40 % [a]	60±4 %	70±10 %	about 60 %

a)   40 % + the ash deposited prior to the sampling station at 650 °C.

4.4.2 Deposition as a function of particle size and composition

The deposition efficiency in the convective pass was found to depend predominantly on the particle size. Practically all of the particles coarser than about 10 μm were deposited during Processes B and C, and the deposition efficiency decreased with decreasing particle size. In the size range < 2 μm, the deposition rate was below the detection limit, lower than about 25 % (Figure 4 and Table 2 in paper V; Lind et al., 1997). The deposition efficiency in Process A was also the highest for the coarsest particles. In Processes A and D the particles in the size range > 10 μm were not entirely absent downstream of the convective pass. The variation in the coarse particle deposition efficiency may be related to the differences in the arrangements and geometries of the heat exchanger tubes, as only Processes B and C were taking place at the same plant.

The elemental composition of fly ash particles of given d_{ae} was found to be approximately the same upstream and downstream of the convective pass in Processes B and C (Figure 8, Figure 4 in Paper V; Lind et al., 1997). This indicates that the deposition efficiency is approximately the same for all the particles with the same d_{ae} regardless of their composition. The deposition efficiency of a species depends predominantly on its particle size. Silicon was deposited most efficiently (90–95 % in Processes B and C), since Si was enriched in the largest particles (Figure 7 in Paper IV). Calcium was present only in the coarse mode particles, but was not so much enriched in the largest particles as Si was. The deposition efficiency of Ca was about 70 % in Process B

and 80 % in Process C. Alkali metals were enriched in the fine particles, which resulted in a lower deposition efficiency compared to that of Ca. Na was present, on average, in coarser particles than K (Figure 6 in Paper IV). The deposition efficiency of Na was correspondingly higher (49–58 % in Process B and 71–74 % in Process C) than that of K (28–41 % in Process B and 62–64 % in Process C). The deposition efficiency of the alkali sulphate fine particles was clearly lower than that of the non-volatile species, e.g. of the Ca-compounds. The sulphate concentration in the sub-micron particles was not decreased between the sampling stations in Process A (27 mg/Nm^3 at 650 °C and 30 mg/Nm^3 at 160 °C). No significant difference in the sub-micron sulphur concentrations was observed between the two sampling stations in Processes B and C.
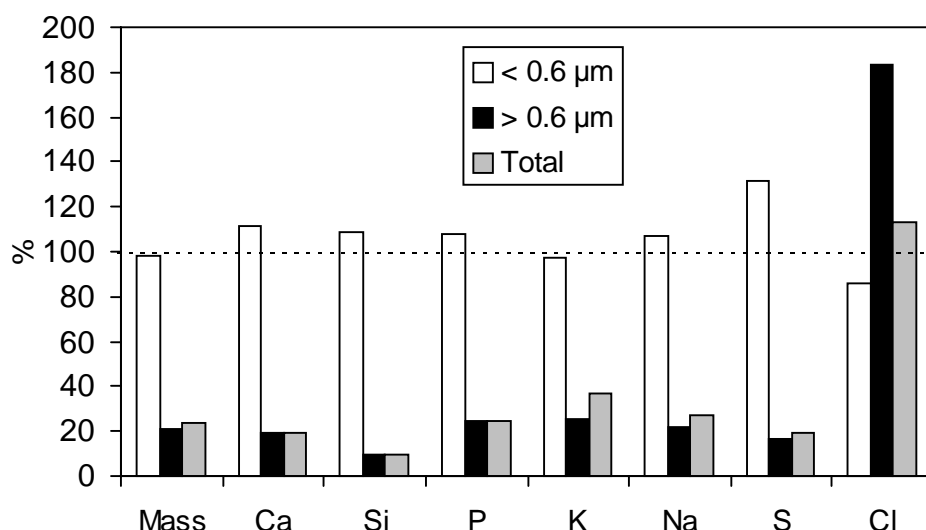

Figure 8. Ratio of concentration downstream of the convective pass to that upstream of the convective pass in combustion of forest residue (Process C).

The deposition efficiency of sulphur depends on the extent of its reactions with Ca and alkali metals. CaSO$_4$ is present almost entirely in the coarse particles, since Ca is not significantly volatilised. On the other hand, alkali sulphates are enriched in fine particles and are not effectively deposited. The different form of sulphur in forest residue ash (predominantly CaSO$_4$) as compared to willow ash (predominantly K$_2$SO$_4$) resulted in very different sulphur deposition behaviour.

The concentration of deposited S was 45–50 mg/Nm^3 during combustion of forest residue, but at most a few mg/Nm^3 during combustion of willow in the same power plant.

The deposition efficiency of the alkali chlorides, that entered the convective pass as vapours, was also much lower than that of the non-volatile species. This can be seen from the fact that the observed total Cl concentration in the ash was not decreased between the sampling stations in Processes B and C (Table 2 in Paper V, Lind et al., 1997). The deposition efficiencies of alkali metals thus depend on their chemical behaviour. Alkali silicates are among the most effectively depositing species due to their large particle size, whereas alkali sulphates and chlorides have a low deposition efficiency.

4.4.3 Effect of coarse particle shape on deposition efficiency

It is possible that particle shape, in addition to particle size, has a significant effect on deposition efficiency. The coarse fly ash particles from wood combustion are much less spherical compared to, for instance, those formed during pulverised coal combustion.

The collision rate on the heat exchanger tubes by impaction is lower for a non-spherical particle than for a sphere with the same mass. This is due to the fact that the non-spherical particle has a smaller d_{ae},

$$d_{ae} = d_{ev} \sqrt{\frac{\rho_p}{1 \, \text{g/cm}^3 \cdot \chi}} \, , \qquad\qquad (31)$$

where d_{ev} is the equivalent volume diameter (diameter of a sphere having the same volume as the particle) and χ is the dynamic shape factor of the particle (Hinds, 1999). The value of χ is 1 for spheres and > 1 for the other shapes (except for some streamlined shapes having a favourable orientation). For instance, $\chi = 1.68$ for a chain consisting of 10 spheres, averaged over all particle orientations (Dahneke, 1982), resulting in a value of d_{ae} 23 % lower than the d_{ae} of a spherical particle with the same volume and density.

The sticking efficiency (probability that a particle is retained on the surface upon collision) is presumably greater for a highly non-spherical particle having a large number of contact points with the target than for a sphere. Apparently, the high sticking efficiency due to particle shape explains the large deposition rate of the coarse particles. However, the data presented here is not sufficient to come to a conclusion about this. Viscosities of the target surface and of the particle also affect the sticking efficiency.

4.5 Alkali chloride condensation

The condensation of alkali chloride vapours may take place on the alkali sulphate fine particles, on the coarse fly ash particles and on the surfaces of heat exchangers and other structures. Alternatively, alkali chlorides may form new, ultrafine particles via homogenous nucleation. Figure 9 shows fine mode particles rich in alkali sulphates and chlorides.
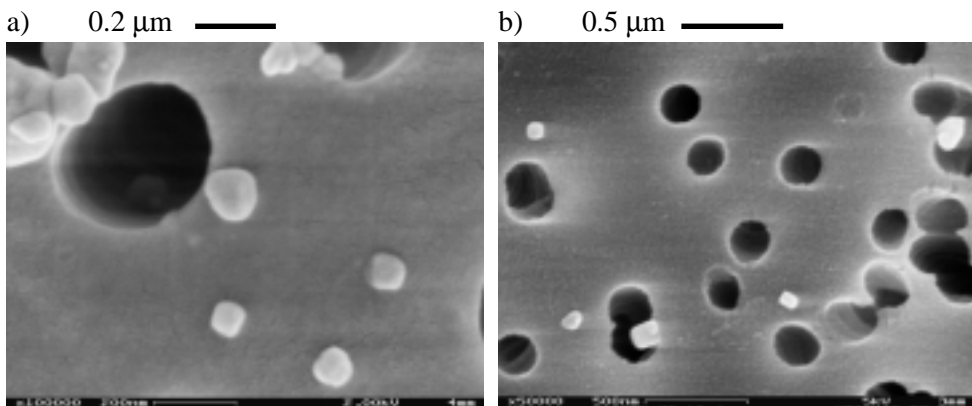
Figure 9. SEM-micrographs of fine mode fly ash particles. a) alkali sulphate-rich particles (willow and wood pellets, Process A) and b) alkali chloride-rich particles (forest residue, Process C). Samples were collected downstream of the convective pass.

In the following, the effect of size distribution of the pre-existing particles on the condensation of alkali chlorides is discussed. The condensation rate on coarse particles was found to be proportional to $1/d_{ae}^{x}$, where $x = 1$–1.2 (Lind, 1999). In the case of spherical particles, x should be equal to 2 (Linak and Wendt, 1993). The value of x was lower than 2 here due to the agglomerated structure of the

particles. Because of the non-spherical shape of the coarse particles, alkali chlorides were condensed on larger particles than they would have been if the coarse particles were spherical. Still, alkali chlorides were not present to a significant extent in the most effectively deposited size fraction, $d_{ae} > 10$ μm (Figure 10 and Figure 5 in Paper V). The efficiency of a coarse particle at collecting vapour via condensation can be determined as

$$
\begin{aligned}
&\frac{M_{cv}}{M} \propto \frac{1}{d_{ae}^{x}}, \\
&\Rightarrow M_{cv} \propto \frac{M}{d_{ae}^{x}},
\end{aligned}
\tag{32}
$$

where M_{cv} is the mass of the condensed vapour present in a particle with a total mass of M. The efficiency of all the coarse particles in a gas volume v at collecting vapour is, correspondingly, proportional to $\Sigma(M/d_{ae}^{x})/v$, where the summation includes all the coarse particles. On the other hand, equation (5) shows that the efficiency of the fine particles at collecting vapour is proportional to $\Sigma(d^2)/v$, if the particles are large enough for $p - p_d \approx p - p_s$. This time the summation includes all the fine particles in the gas volume v. In practice, $\Sigma(d^2)/v$ cannot be calculated, as the particle number size distribution in the region where the alkali chloride condensation occurs is not known. The most closely related quantity that can be estimated is the mass concentration, or $\Sigma(\rho_p d^3)/v$, both before any condensation of the alkali chlorides has taken place as well as after condensation has finished.

The fine mode mass concentration was clearly lower during combustion of forest residue than in willow combustion (Table 7). On the other hand, the value of $\Sigma(M/d_{ae})/v$ for the coarse particles was higher in the case of forest residue combustion. As expected, under these circumstances a larger fraction of Cl was found in the fine mode particles in the case of willow than in the case of forest residue burned at the same power plant (69 % vs. 49 %). An extensive formation of alkali sulphates increases the fraction of alkali chlorides condensing on the fine particles, and thus lowers the alkali chloride deposition efficiency. The data from Process A is in agreement with this result, although Process A, which took place at a different plant, cannot be compared directly to the other processes. This is due to the possibly different coarse particle deposition rate, which affects

the amount of alkali chlorides found in the coarse particles downstream of the convective pass.
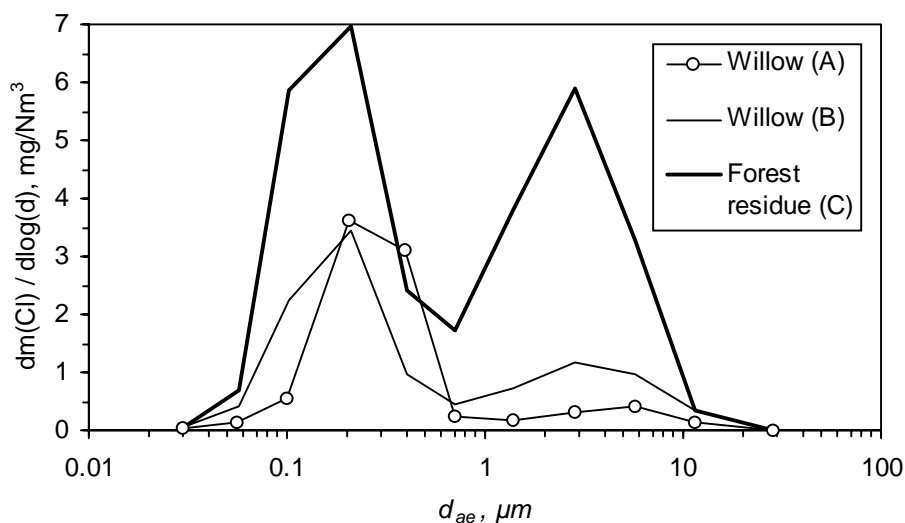
Figure 10. Mass size distribution of Cl in the fly ash downstream of the convective pass. The behaviour of Cl represents that of the alkali chlorides, as Cl is expected not to be present to a significant extent in any other condensed form as alkali chlorides.

Table 7. Fraction of Cl in the fine mode particles of all the Cl observed in the fly ash downstream of the convective pass. The mass concentration of the fine particle mode, as well as $\Sigma(M/d_{ae}^{x})/v$ upstream of the convective pass are also shown.

Process	Fine mode, mg/Nm³		$\Sigma(M/d_{ae})/v$,	Cl in the
	Without chlorides	total	(mg/µm)/Nm³	fine mode, %
Willow (A)	48 [a,b]	53 [a]	180–230 [a,c]	85
Willow (B)	34	39	179	69
Forest residue (C)	4	20	269	49

[a]) Total mass concentration at the sampling station at 650 °C.

[b]) KCl - concentration is based on the data at 160 °C.

[c]) The indicated inaccuracy is due to the fact that d_{ae} for the pre-cyclone collected particles is not accurately known.

4.6 Discussion on the alkali chloride superheater deposition mechanisms

The deposition efficiency of alkali chlorides was found to be definitely lower than that of the coarse silicate-rich particles. However, in some cases, alkali chlorides are enriched in the inner layers of the superheater deposits, as discussed in the Section 2.5.2. This indicates that the information about deposition efficiency alone is inadequate for understanding the deposit formation mechanism. The physical form of the depositing species is also important when the behaviour after the initial deposition is studied. Coarse particles are deposited on top of the deposit layer, and are likely to fall off the layer, or become removed during the soot-blowing. The fine particles travel towards the tube surface, driven by thermophoresis, until they collide with the previously deposited particles. Vapours are driven towards the tube surface by diffusion. The vapours are, unlike the rectilinearly moving particles, able to penetrate through the deposit, as far as it is porous. The vapour condensation begins at the region where $p_s / p = 1$.

Alkali silicates are present in the superheater section in the coarse fly ash particles. Alkali sulphates are present predominantly in the fine particles, and to a lesser extent also in the coarse particles. On the other hand, the physical form in which alkali chlorides are deposited on the superheater surfaces is not definite. In the superheater section ($T_\infty \approx 800$ °C), alkali chlorides are present as vapour outside the thermal boundary layer of the superheater tubes (unless their mass concentration exceeds ≈ 1 g/m^3). However, the deposition of alkali chlorides does not necessarily take place predominantly via vapour condensation if the gas temperature at the outer deposit surface is below the dew point. The alkali chloride vapour may condense on the ash particles or form new particles via nucleation as the gas temperature decreases while the vapour is transported through the thermal boundary layer. In the following, an order-of-magnitude analysis is presented to estimate whether the residence time in the boundary layer is long enough for the condensation of supersaturated alkali chloride vapour on the ash particles in the thermal boundary layer.

The average penetration time ($t_{bl,v}$) of a vapour molecule in a thermal boundary layer of thickness X can be estimated using the average velocity of a vapour

molecule in the diffusion boundary layer ($V_{bl,v}$), which can be obtained from equation (10),

$$t_{bl,v} \approx \frac{X}{V_{bl,v}} \approx \frac{X}{\dot{m}_{d,v}/m_v} = \frac{X \cdot D_t}{D_v \cdot \mathrm{Sh}} . \tag{33}$$

The thickness of the thermal boundary layer of the superheater tubes is of the order of 1 mm, as estimated by calculating $(T_\infty – T_w)/\nabla T$ from equation (18). This results in a value of $t_{bl,v}$ of the order of 0.01 seconds. The consumption rate of the supersaturated vapour by condensation on monodisperse fine particles can be estimated by presenting equation (5) in the following form:

$$\frac{dm_{ssat}}{dt} = -\frac{\sqrt{\eth} \cdot RT_0 N d^2 \alpha}{\sqrt{2kTM_{mol,v} N_a}} \cdot m_{ssat} ,$$

$$m_{ssat} = m - m_d , \tag{34}$$

where m_{ssat} is the mass concentration of the supersaturated vapour, N is the particle number concentration normalised using a reference temperature T_0 ($T_0 = 273$ K when N is given in particles/Ncm^3), m is the total mass concentration of the vapour, and m_d is the mass concentration corresponding to the saturation vapour pressure p_d (equation 8). For an order-of-magnitude analysis, m_d and T can be considered to be constants, having the values prevailing at the tube surface.

Neglecting the fact that the particles grow due to condensation (that is assuming that the vapour mass concentration is small compared to the particle mass concentration), the fraction of the supersaturated vapour not yet condensed after time t can be calculated from

$$\frac{m_{ssat}(t)}{m_{ssat}(t=0)} = \exp\left(\frac{t}{m_{ssat}} \cdot \frac{dm_{ssat}}{dt} \right) ,$$

$$= \exp\left(-t \frac{\sqrt{\eth} \cdot RT_0 N d^2 \alpha}{\sqrt{2kTM_{mol,v} N_a}} \right) . \tag{35}$$

The fine mode particle concentration prior to alkali chloride condensation was at the most 48 mg/Nm^3 (Table 7). The concentration of 48 mg/Nm^3 corresponds to, for instance, 10^8 particles/Ncm^3 with $d = 0.07$ µm, or 10^7 particles/Ncm^3 with $d = 0.15$ µm. Assuming • $= 1$, the fraction of the supersaturated KCl monomer that has condensed on the alkali sulphate particles in 0.01 seconds at $T = 550$ °C is 46 % or 25 %, respectively. For the dimer, $(KCl)_2$, the condensed fractions are slightly lower (35 % or 18 %) due to the twofold value of $M_{mol,v}$. Assuming • $= 0.04$, the respective condensed fractions are only 1–2 %.

According to the order-of-magnitude estimate, it is possible that a significant fraction of the alkali chloride vapour is condensed in the thermal boundary layer, at least if T_∞ is only slightly above the dew point. The dominant physical form (vapour, fine particles or coarse particles) of the alkali chlorides depositing on the superheater surfaces depends on the local circumstances in the vicinity of the tube surface. The important factors include concentration and size distribution of the pre-existing fly ash particles, the concentrations of alkali chlorides and the temperature field in the boundary layer.

5. Conclusions

The behaviour of alkali metals, especially potassium, during combustion of wood-based fuels was studied in pilot and industrial scale CFBC - boilers. A simplified picture of the chemical and physical transformations of potassium is shown in Figure 11. The transformation mechanisms were determined, based on the results of this work as well those of Bryers (1996), Christensen and Livbjerg (1996), Christensen et al. (1998), Dayton et al. (1995), French and Milne (1994), Latva-Somppi (1998), Latva-Somppi et al. (1998a), Lind (1999) and Manzoori and Agarwal (1992, 1993).

Up to 40 % of the ash-forming constituents were retained in the bed and were removed with the bottom ash. The chemical reaction between the potassium compounds and the bed material resulted in enrichment of K in the bottom ash ($BF(K) / BF(Ca)$ = 1.12–1.4) when the Si content of fuel was below 0.2 %. However, potassium was not enriched in the bottom ash ($BF(K) / BF(Ca)$ = 0.43) when the fuel Si content was 2.6 % (wood and paper mill sludge), as the reaction of K with the fuel-originated quartz and silicates dominated over the reaction with the bed material.

The fly ash released from the combustion chamber includes K as KCl-vapour, K_2SO_4 fine particles (< 1 µm) and K in the coarse particles (1–100 µm), mainly as silicates. The fine particles upstream of the convective pass consist almost entirely of alkali sulphates, whereas the coarse particles contain all the non-volatile species (e.g. Si, Ca and P). The fraction of potassium present as sulphates and chlorides of all the potassium in the fly ash was found to be the higher the lower the Si to K ratio in the fuel was. The increased amount of Si in the fuel increases the extent of the alkali silicate formation, resulting in a decrease in the mass concentrations of K_2SO_4 and KCl. This correlation was obtained for processes with sulphur and chlorine in excess of the amount needed to bind all the K and Na to chlorides and sulphates. The correlation is valid only as far as the combustion temperature and the fuel moisture do not deviate remarkably from the values in the studied processes ($\approx$ 800 °C and $\approx$ 50 %, respectively).

Fragmented bed material in coarse fly ash, incl. K-silicates.

Coarse fly ash, incl. K-silicates, K_2SO_4, KCl (and K_2CO_3).

Fine fly ash enriched with K_2SO_4, KCl (and K_2CO_3).

Sulfation (and carbonisation)

Condensation

Condensation

Condensation

Convective pass

Combustion chamber

KCl(g)   KOH(g)

Recirculation back to bed

SO_2 release

Attachment

K_2SO_4 - rich fine particles

$+ SO_2$ (g)

SiO_2 + K-silicates

Attachment

SiO_2 + K-silicates

Attachment

Ash, incl. K-silicates and K_2SO_4

KCl(g) KOH(g)

Attached ash reacts with quartz.

KCl (g), KOH (g), K_2SO_4 (g)

Reaction with quartz

Bed particle (SiO_2)

Fuel particles, K as salts, in organic form and as K-silicates.

Figure 11. Behaviour of potassium during circulating fluidised bed combustion of biomass.

78

Alkali chlorides were condensed on the fly ash particles in the convective pass. The fraction condensed on the fine-mode particles was 49–85 %, the rest condensed on the coarse particles. The fine-mode fraction increased as the mass concentration of the alkali sulphate particles increased, and as the quantity $\Sigma(M/d_{ae})/v$ of the coarse particles decreased.

About 60–70 % of the fly ash entering the convective pass was deposited on the heat exchanger surfaces, when the soot-blowing was not carried out. Thus, it is proposed that the soot-blowing periods are of considerable interest when the performance of the gas-cleaning devices and fly ash emissions during the combustion of wood are studied. The reason for a deposition efficiency much higher than that of the coal fly ash cannot be concluded based on the data presented here. It is conceivable, however, that the highly agglomerate structure of the coarse ash particles might have resulted in an increased sticking efficiency of the impacting particles due to the increased number of contact points with the target. The deposition efficiency correlated clearly with the ash particle size. The largest particles, including alkali silicates, were deposited most effectively, and the deposition efficiency decreased with decreasing particle size. The deposition efficiency of the fine mode particles was below the detection limit (less than about 25 %). The deposition efficiencies of alkali chlorides and sulphates were also less than about 25 %, as they were not present to a significant extent in the size fraction $d_{ae} > 10$ µm. The deposition efficiencies of particles with the same d_{ae} but varying composition were not found to be different.

The effect of the porous outer deposit layer of impacted coarse particles on protecting the superheater tube requires further study. In the case where the alkali and Cl species are not able to penetrate through the outer layer, the alkali-rich layers sometimes observed near the tube surface (below the porous layer) must grow mainly during the periods soon after soot-blowing before the porous outer layer grows again. The enrichment of Cl in the superheater deposits observed elsewhere (Miles et al., 1996) is proposed to be a consequence of inefficient cleaning of the innermost Cl-rich deposit layers during the periodic soot-blowings. The outer layers, enriched with impacted coarse particles that are depleted in Cl, are more easily removed. Also, the direct reaction of HCl on the heat exchanger surfaces may contribute to the enrichment of chlorine in the deposits. Cl was found to be released from the furnace mainly in gaseous form, according to the mass balance calculations on Processes B and C. For future

work, it is a challenging task to find out under what circumstances the chlorine-assisted corrosion is predominantly caused by KCl, and when by gaseous Cl species (e.g. HCl). Also, it is of interest to find out if the physical form of the depositing KCl (vapour, fine particles or coarse particles) is important with regard to the extent of the corrosion problems.

The behaviour of sulphur varied extensively between the fuels. About 99 % of the condensed-phase sulphur was present in the coarse particles ($CaSO_4$) during combustion of forest residue, whereas in the case of willow a majority of it was present as K_2SO_4 in the fine particles. Correspondingly, during combustion of willow, less than 20 % of the condensed-phase S was deposited in the convective pass whereas, with the forest residue, the efficiency was about 80 %. The extent of sulphation of CaO on the superheater deposit layer is proposed as of interest for further study. The sulphation of CaO would reduce the amount of SO_2 and SO_3 available for reaction with KCl and NaCl. This effect would be important, especially in combustion of wood fuels, as Ca is typically the most common ash-forming element in wood.

In order to better predict and minimise the extent of superheater corrosion during the FBC of wood-based fuels, present knowledge about the deposition mechanisms of different ash species should be linked to the knowledge of the structure of actual deposit layers observed in power plants. This would require laboratory-scale research under well-known process conditions, as well as deposition probe experiments in power plants combined with detection of the concentrations and forms of the inorganic species upstream of the superheater section.

References

Anthony, E.J. (1995). Fluidized bed combustion of alternative solid fuels; status, successes and problems of the technology. *Prog. Energy Combust. Sci.*, **21**, pp. 239–268.

Bale, C.W., Pelton, A.D. and Thompson, W.T. (1996). F*A*C*T 2.1. User Manual. Ecole Polytechnique de Montreal / Royal Military College, Canada.

Baxter, L. L., Miles, T.R., Miles, T.R. Jr., Jenkins, B.M., Milne, T., Dayton, D., Bryers, R.W. and Oden, L.L. (1998). The behavior of inorganic material in biomass-fired power boilers: field and laboratory experiences. *Fuel Processing Technology*, **54**, pp. 47–78.

Biswas, P. and Flagan, R.C. (1984). High-Velocity Inertial Impactors. *Environ. Sci. Technol.* **18**, pp. 611–616.

Biswas, P., Jones, C.L. and Flagan, R.C. (1987). Distortion of size distributions by condensation and evaporation in aerosol instruments. *Aerosol. Sci. Technol.* **7**, pp. 231–246.

Biswas, P., Li X. and Pratsinis, S.E. (1989). Optical waveguide preform fabrication: Silica formation and growth in a high temperature aerosol reactor. *J. Appl. Phys.* **65(6)**, pp. 2445–2450.

Bryers, R.W. (1996). Fireside slagging, fouling and high-temperature corrosion of heat-transfer surface due to impurities in steam-raising fuels. *Prog. Energy Combust. Sci.,* **22**, pp. 29–120.

Castillo, J.L. and Rosner, D.E. (1988). A nonequilibrium theory of surface deposition from particle-laden, dilute condensible vapor-containing laminar boundary layers. *Int. J. Multiphase Flow*, **14**, pp. 99–120.

Christensen, K.A. and Livbjerg, H. (1996). A field study of submicron particles from the combustion of straw. *Aerosol Sci. Tech.*, **25**, pp. 189–199.

Christensen, K.A., Stenholm, M. and Livbjerg, H. (1998). The formation of submicron aerosol particles, HCl and SO_2 in straw-fired boilers. *J. Aerosol Sci.*, **29**, pp. 421–444.

Dahl, J. and Obernberger, I. (1998). Fractionated heavy metal separation. 2nd Annual Report for CEC in project JOR3-CT950001.

Dahneke, B.A. (1982). Viscous Resistance of Straight-Chain Aggregates of Uniform Spheres. *Aerosol Sci. Tech.*, **1**, pp. 179–185.

Dayton, D.C., Belle-Oudry, D. and Nordin, A. (1999a). Effect of Coal Minerals on Chlorine and Alkali Metals Released during Biomass/Coal Cofiring. *Energy & Fuels*, **13**, pp. 1203–1211.

Dayton, D.C., French, R.J. and Milne, T.A. (1995). Direct Observation of Alkali Vapor Release during Biomass Combustion and Gasification. 1. Application of Molecular Beam/Mass Spectrometry to Switchgrass Combustion. *Energy & Fuels*, **9**, pp. 855–865.

Dayton, D.C., Jenkins, B.M., Turn, S.Q., Bakker, R.R., Williams, R.B., Belle-Oudry, D. and Hill, L.M. (1999b). Release of Inorganic Constituents from Leached Biomass during Thermal Conversion. *Energy & Fuels*, **13**, pp. 860–870.

Dayton, D.C. and Milne, T.A. (1996). Laboratory measurements of alkali metal containing vapors during biomass combustion. In: Applications of Advanced Technology to Ash-Related Problems in Boilers. Ed. by Baxter, L. and DeSollar, R. Proceedings of the Engineering Foundation Conference, Waterville Valley, USA 16–21 July 1995. Plenum Press, New York. Pp. 161–185.

Energiakatsaus 2/99 (1999). Ministry of Trade and Industry, Finland. In Finnish. 44 p.

Erickson, T.A., Ludlow, D.K. and Benson, S.A. (1992). Fly ash development from sodium, sulphur and silica during coal combustion. *Fuel*, **74**, pp. 615–622.

Flagan, R.C. and Seinfeld, J.H. (1988). *Fundamentals of air pollution Engineering.* Prentice-Hall, Englewood Cliffs, NJ. 542 p.

French, R.J. and Milne, T.A. (1994). Vapor phase release of alkali species in the combustion of biomass pyrolysis oils. *Biomass and Bioenergy*, **7**, pp. 315–325.

Hall, D.O., Rosillo-Calle, F., Williams, R.H. and Woods, J. (1993). Biomass for energy: Supply prospects. In: Renewable Energy: Sources for Fuels and Electricity. Ed. by Johansson, T.B., Kelly, H., Reddy, A.K.N., Williams, R.H. and Burnham, L. Island Press, Washington, D.C. Pp. 593-651.

Helynen, S. and Nousiainen, I. (1996). Biopolttoaineiden tuotanto- ja käyttöpotentiaalit. Ministry of Trade and Industry, Finland. In Finnish. 114 p.

Hering, S.V. (1987) Calibration of the QCM impactor for Stratospheric Sampling. *Aerosol. Sci. Technol.* **7**, pp. 257–274.

Hernberg, R., Stenberg, J. and Zethraeus, B. (1993). Simultaneous in-situ measurement of temperature and size of burning char particles in a fluidized bed furnace by means of fiber optic pyrometry. *Combustion & Flame*, **95**, pp. 191–205.

Heyder J., Gebhart, J., Rudolf, G., Schiller, C. F. and Stahlhofen, W. (1986) Deposition of particles in the human respiratory tract in the size range 0.005-15 μm. *J. Aerosol Sci.* **17**, pp. 811–825.

Hillamo, R.E. and Kauppinen, E.I. (1991). On the performance of the Berner Low Pressure Impactor. *Aerosol Sci. Technol.* **14**, pp. 33–47.

Hinds, W.C. (1999). Aerosol Technology. Properties, Behavior, and Measurement of Airborne Particles. 2nd ed. Wiley-Interscience, New York. 483 p.

Iisa, K., Lu, Y. and Salmenoja, K. (1999). Sulfation of Potassium Chloride at Combustion Conditions. *Energy & Fuels*, **13**, pp. 1184–1190.

International Energy Agency (1998). Energy statistics of OECD countries, 1995–1996. Paris, France.

Jensen, P.A., Stenholm, M. and Hald, P. (1997). Deposition Investigation in Straw-Fired Boilers. *Energy and Fuels*, **11**, pp. 1048–1055.

Jokiniemi, J.K., Lazaridis, M., Lehtinen, K.E.J. and Kauppinen, E.I. (1994). Numerical simulation of vapour-aerosol dynamics in combustion processes. *J. Aerosol Sci.* **25**, pp. 429–446.

Jokiniemi, J.K., Pyykönen, J., Mikkanen, P. and Kauppinen, E.I. (1996). Modeling fume formation and deposition in kraft recovery boilers. *Tappi Journal* **79**, No. 7, pp. 171–180.

Joutsensaari, J., Kauppinen, E.I., Jokiniemi, J.K. and Helble, J.J. (1994). Studies on ash vaporization in power plant scale pulverized coal combustion. In: The Impact of Ash Deposition on Coal Fired Plant. Ed. by Williamson, J. and Wigley, F. Proceedings of the Engineering Foundation Conference, Solihull, UK 20–25 June 1993. Taylor & Francis. Pp. 613–624.

Kauppinen, E. I. (1992). On the determination of continuous submicrometer liquid aerosol-size distributions with low pressure impactors. *Aerosol Sci. Technol.* **16**, pp. 171–197.

Kauppinen, E.I. and Pakkanen T.A. (1990). Coal Combustion Aerosols: A Field Study. *Environ. Sci. Technol.* **24**, pp. 1811–1818.

Koch, W., Lödding, H., Mölter, W. and Munzinger, F. (1988). Verdünnungssystem für die Messung hochkonzentrierter Aerosole mit optischen Partikelzählern. *Staub-Reinhaltungen der Luft*. **48**, pp. 341–344.

Kunii, D. and Levenspiel, O. (1991). *Fluidization Engineering*. 2nd ed. Butterworth-Heinemann series in Chemical Engineering, Boston, USA. 491 p.

Latva-Somppi, J. (1998). Experimental studies on pulp and paper mill sludge ash behavior in fluidized bed combustors. PhD thesis. Technical Research Centre of Finland, Espoo. VTT Publications 336. 89 p. + app. 86 p.

Latva-Somppi, J., Kurkela, J., Tapper, U., Kauppinen, E.I., Jokiniemi J.K. and Johanson B. (1998a). Ash deposition on bed material particles during fluidized bed combustion of wood-based fuels. Proceedings of the International Conference on Ash Behavior Control in Energy Conversion Systems, Yokohama, Japan. Pp. 119–126.

Latva-Somppi, J., Kauppinen, E.I., Kurkela, J., Tapper, U., Öhman, M., Nordin, A. and Johanson B. (1998b). Ultrafine ash particle formation during waste sludge incineration in fluidized bed reactors. *Combust. Sci. and Technol.*, **134**, pp. 433–455.

Leckner, B. (1998). Fluidized bed combustion: Mixing and pollutant limitation. *Prog. Energy Combust. Sci.*, **24**, pp. 31–61.

Linak, W.P. and Wendt, J.O.L. (1993). Toxic metal emissions from incineration: Mechanisms and control. *Prog. Energy Combust. Sci*., **19**, pp. 145–185.

Lind, T. (1999). Ash formation in circulating fluidised bed combustion of coal and solid biomass. PhD thesis. Technical Research Centre of Finland, Espoo. VTT Publications 378. 80 p. + app. 83 p.

Lind, T., Kauppinen, E.I., Jokiniemi, J.K., Maenhaut, W. and Pakkanen, T.A. (1994). Alkali metal behaviour in atmospheric circulating fluidised bed coal combustion. In: The Impact of Ash Deposition on Coal Fired Plant. Ed. by Williamson, J. and Wigley, F. Proceedings of the Engineering Foundation Conference, Solihull, UK 20–25 June 1993. Taylor & Francis. Pp. 77–88.

Lind, T., Kauppinen, E.I., Maenhaut, W., Shah, A. and Huggins, F. (1996). Ash Vaporization in Circulating Fluidized Bed Coal Combustion. *Aerosol Sci. Tech.*, **24**, pp. 135–150.

Lind, T., Kauppinen, E.I., Sfiris, G., Nilsson, K. and Maenhaut, W. (1999). Fly Ash Deposition Onto the Convective Heat Exchangers During Combustion of Willow in a Circulating Fluidized Bed Boiler. In: Impact of Mineral Impurities in Solid Fuel Combustion. Ed. by Gupta R.P., Wall, T.F. and Baxter, L. Kluwer Academic / Plenum Publishers, New York, N.Y. Pp. 541–553.

Lyngfelt, A., Åmand, L.-E. and Leckner, B. (1996). Progress of combustion in the furnace of a circulating fluidised bed boiler. Twenty-sixth International Symposium on Combustion. The Combustion Institute, Pittsburgh, USA. Pp. 3253–3260.

Manzoori, A.R. and Agarwal, P.K. (1992). The fate of organically bound inorganic elements and sodium chloride during fluidized bed combustion of high sodium, high sulphur low rank coals. *Fuel,* **71**, pp. 513–522.

Manzoori, A.R. and Agarwal, P.K. (1993). The role of inorganic matter in coal in the formation of agglomerates in circulating fluid bed combustors. *Fuel*, **72**, pp. 1069–1075.

McElroy, M.W., Carr, R.C., Ensor, D.S. and Markowski, G.R. (1982) Size Distribution of Fine Particles from Coal Combustion. *SCIENCE* **215**, pp. 13–19.

Michelsen, H.P., Frandsen, F., Dam-Johansen, K. and Larsen, O.H. (1998). Deposition and high temperature corrosion in a 10 MW straw fired boiler. *Fuel Processing Technology,* **54**, pp. 95–108.

Miles, T.R., Miles, T.R. Jr., Baxter, L.L., Bryers, R.W., Jenkins, B.M. and Oden, L.L. 1996. Boiler Deposits from Firing Biomass Fuels. *Biomass and Bioenergy*, **10**, pp. 125–138.

Neville, M. and Sarofim, A.F. (1985). The fate of sodium during pulverized coal combustion. *Fuel*, **64**, pp. 384–390.

Nielsen, H.P., Frandsen, F.J. and Dam-Johansen, K. (1999). Lab-Scale Investigations of High-Temperature Corrosion Phenomena in Straw-Fired Boilers. *Energy & Fuels*, **13**, pp. 1114–1121.

Nordin, A. (1994). Chemical elemental characteristics of biomass fuels. *Biomass and Bioenergy*, **6**, pp. 339–347.

Nordin, A. (1995). Optimization of sulfur retention in ash when cocombusting high sulfur fuels and biomass fuels in a small pilot scale fluidized bed. *Fuel*, **74**, pp. 615–622.

Parker, R., Calvert, S., Drehmel D. and Abbott J. (1981). Inertial Impaction of Fine Particles at High Temperature and High Pressure. *J. Aerosol Sci.* **12**, pp. 297–306.

Perry's Chemical Engineers' Handbook (1984). Ed. by Perry, R.H., Green D.W. and Maloney, J.O. 6th ed., McGraw–Hill, New York.

Pope, C.A. III, Thun, M.J., Namboodiri, M.M., Dockery, D.W., Evans, J.S., Speizer, F.E. and Heath Jr., C.W. (1995). Particulate air pollution as a predictor of mortality in a prospective study of U.S. adults. *American Journal of Respiratory and Critical Care Medicine* **151**, pp. 669–674.

Porle, K., Klippel, N., Riccius, O., Kauppinen, E.I. and Lind, T. (1995). Full scale ESP performance after PC-boilers firing low sulfur coals. *EPRI/DOE International Conference on Managing Hazardous and Particulate Air Pollutants, August 15–17, 1995*. Toronto, Ontario, Canada.

Pyykönen, J., Jokiniemi, J.K. and Jacobson, T. (1999) Development of a Prediction Scheme for Pulverised Coal-Fired Boiler Slagging. In: Impact of Mineral Impurities in Solid Fuel Combustion. Ed. by Gupta R.P., Wall, T.F. and Baxter, L. Kluwer Academic / Plenum Publishers, New York, N.Y. Pp. 735-752.

Quann, R.J. and Sarofim, A.F. (1982) Vaporization of refractory oxides during pulverized coal combustion. Nineteenth International Symposium on Combustion. The Combustion Institute, Pittsburgh, PA. Pp. 1429–1440.

Raask, E. (1985). *Mineral Impurities in Coal Combustion*. Hemisphere Publishing, Washington. 484 p.

Rader, D.J. and Marple, V.A. (1985). Effect of ultra-Stokesian drag and particle interception on impaction characteristics. *Aerosol. Sci. Technol.* **4**, pp. 141–156.

Rosner, D.E. (1986). *Transport Processes in Chemically Reacting Flow Systems*. Butterworth-Heinemann, Boston. 540 p.

Sander, B. (1997). Properties of Danish biofuels and the requirements for power production. *Biomass and Bioenergy*, **12**, pp. 177–183.

Sarofim, A.F. and Helble, J.J. (1994). Mechanisms of Ash and Deposit Formation. In: The Impact of Ash Deposition on Coal Fired Plant. Ed. by Williamson, J. and Wigley, F. Proceedings of the Engineering Foundation Conference, Solihull, UK 20–25 June 1993. Taylor & Francis. Pp. 567–582.

Skrifvars, B-J., Backman, R., Hupa, M., Sfiris, G., Åbyhammar, T. and Lyngfelt, A. (1998). Ash behaviour in a CFB boiler during combustion of coal, peat or wood. *Fuel*, **77**, pp. 65–70.

Seinfeld, J.H. and Pandis, S.N. (1998). *Athmospheric Chemistry and Physics.* Wiley, New York. 1326 p.

Steinberg, M. and Schofield, K. (1990). The chemistry of sodium with sulfur in flames. *Prog. Energy Combust. Sci.*, **16**, pp. 311–317.

Tran, H. (1997). Recovery boiler corrosion. In: Kraft recovery boilers. Ed. by Adams, T.N. TAPPI Press, Atlanta, GA, USA. Pp. 285–324.

Waldmann, L. and Schmitt, K.H. (1966). Thermophoresis and diffusiophoresis of aerosols. In: Aerosol Science. Ed. by Davies, C.N., Academic Press, London.

Wessel, R.A. and Righi, J. (1988). Generalized correlations for inertial impaction of particles on a circular cylinder. *Aerosol Sci. Tech.*, **9**, pp. 29–60.

Wibberley, L.J. and Wall, T.F. (1982a). Alkali-ash reactions and deposit formation in pulverized-coal-fired boilers: the thermodynamic aspects involving silica, sodium, sulphur and chlorine. *Fuel*, **61**, pp. 87–92.

Wibberley, L.J. and Wall, T.F. (1982b). Alkali-ash reactions and deposit formation in pulverized-coal-fired boilers: experimental aspects of sodium silicate formation and the formation of deposits. *Fuel*, **61**, pp. 93–99.

Wornat, M.J., Hurt. R.H., Yang, N.Y.C. and Headley, T.J. (1995). Structural and Compositional Transformations of Biomass Chars during Combustion. *Combustion and Flame,* **100**, pp. 131–143.

Appendices of this publication are not included in the PDF version. Please order the printed version to get the complete publication (http://otatrip.hut.fi/vtt/jure/index.html)

Author(s)
Valmari, Tuomas

Title

Potassium behaviour during combustion of wood in circulating fluidised bed power plants

Abstract

The behaviour of potassium during circulating fluidised bed combustion of wood-based fuels was studied experimentally in pilot-scale and industrial scale combustors. Aerosol measurement techniques were used for sampling fly ash and inorganic vapours from the flue gas, upstream and downstream of the convective pass. Elemental analysis methods and scanning electron microscopy were used for sample characterisation. The factors affecting in-duct impactor operation in elevated temperatures are discussed in detail.

The fly ash released from the combustion chamber consisted of i) coarse particles (1–100 • m) that contained all the non-volatile species, including alkali silicates and $CaSO_4$, as well as of ii) sub-micron K_2SO_4 particles. KCl was released from the combustion chamber as vapour, and was condensed on the fly ash particles in the convective pass. The fraction of K ending up in the fly ash as alkali silicates was found to depend on the fuel Si–content. A high fuel Si–content also resulted in depletion of K in the bottom ash. About 60–70 % of the fly ash entering the convective pass was deposited on the heat exchanger surfaces in the convective pass, and was removed during the soot-blowing period. The deposition efficiency correlated clearly with the ash-particle size. The largest particles, including alkali silicates, were deposited most effectively, and the deposition efficiency decreased with decreasing particle size.

The physical state (vapour, fine particle or coarse particle) of the ash species was shown to have a remarkable effect on the form and rate of ash deposition in the convective pass. When the different fuels were compared, the variation in the deposition efficiency was the most remarkable for sulphur.

Author(s)
Valmari, Tuomas

Title

Potassium behaviour during combustion of wood in circulating fluidised bed power plants

Abstract

The behaviour of potassium during circulating fluidised bed combustion of wood-based fuels was studied experimentally in pilot-scale and industrial scale combustors. Aerosol measurement techniques were used for sampling fly ash and inorganic vapours from the flue gas, upstream and downstream of the convective pass. Elemental analysis methods and scanning electron microscopy were used for sample characterisation. The factors affecting in-duct impactor operation in elevated temperatures are discussed in detail.

The fly ash released from the combustion chamber consisted of i) coarse particles (1–100 • m) that contained all the non-volatile species, including alkali silicates and $CaSO_4$, as well as of ii) sub-micron K_2SO_4 particles. KCl was released from the combustion chamber as vapour, and was condensed on the fly ash particles in the convective pass. The fraction of K ending up in the fly ash as alkali silicates was found to depend on the fuel Si–content. A high fuel Si–content also resulted in depletion of K in the bottom ash. About 60–70 % of the fly ash entering the convective pass was deposited on the heat exchanger surfaces in the convective pass, and was removed during the soot-blowing period. The deposition efficiency correlated clearly with the ash-particle size. The largest particles, including alkali silicates, were deposited most effectively, and the deposition efficiency decreased with decreasing particle size.

The physical state (vapour, fine particle or coarse particle) of the ash species was shown to have a remarkable effect on the form and rate of ash deposition in the convective pass. When the different fuels were compared, the variation in the deposition efficiency was the most remarkable for sulphur.

Keywords
biomass, wood, wood fuels, combustion, CFBC, fluidized bed combustion, ashes, alkali metals, potassium, deposition, heat exchangers